Ontogenetic growth in the crania of *Exaeretodon argentinus* (Synapsida: Cynodontia) captures a dietary shift

Brenen Wynd [Corresp., 1], **Fernando Abdala** [2, 3], **Sterling Nesbitt** [1]

[1] Department of Geosciences, Virginia Tech, Blacksburg, Virginia, United States of America

[2] CONICET-Fundación Miguel Lillo, Unidad Ejecutora Lillo, San Miguel de Tucumán, Tucumán, Argentina

[3] Evolutionary Studies Institute, University of the Witwatersrand, Johannesburg, South Africa

Corresponding Author: Brenen Wynd
Email address: bmwynd@vt.edu

Ecological differentiation in vertebrates is a common occurrence where ecology shifts with morphology throughout growth. How ecology shifts over a vertebrate's lifetime is often reconstructed in extant species—by combining observational and skeletal data from growth series of the same species—because interactions between organisms and their environment can be observed directly with little inference. However, reconstructing shifts using extinct vertebrates is difficult and requires well-sampled growth series, specimens with good preservation, and easily observable skeletal traits associated with the specific ecologies. To reconstruct ecological changes through the growth of a stem-mammal, we describe changes associated with dietary ecology in a growth series of crania of the large-bodied (~2 m in length) and herbivorous form, *Exaeretodon argentinus* (Cynodontia: Traversodontidae) from the Late Triassic, Ischigualasto Formation, San Juan, Argentina. Nearly all specimens were deformed by taphonomic processes, so we reconstructed allometric slope using a generalized linear mixed effects model with distortion as a random effect; previous approaches to reconstruct allometry (ordinary least squares or reduced major axis regression) were not used because they are unable to account for additional variation due to fossilization. Under a mixed effects model, we find that through growth, *E. argentinus* reduced the relative length of the palate, postcanine series, orbits, and basicranium, and expanded the relative length of the temporal region and the height of the zygomatic arch. The allometric relationship between the zygomatic arch and temporal region with the total length of the skull approximate the rate of growth for feeding musculature. Based on a higher allometric slope, the zygoma are growing relatively faster than the temporal region. The higher rate of change in the zygoma may suggest that smaller individuals had a crushing-dominated feeding style that transitioned into a chewing-dominated feeding style in larger individuals, suggesting a dietary shift from a lower proportion of plant material to a more plant-dominated diet. Dietary differentiation

through development is further supported by an increase in sutural complexity and a shift in the orientation of microwear anisotropy between small and large individuals of *E. argentinus*. A developmental transition in the feeding ecology of *E. argentinus* is reflective of the reconstructed dietary transition across Gomphodontia, wherein the earliest-diverging species are reconstructed as omnivorous and the well-nested traversodontids are reconstructed as herbivorous. Combining dietary and morphological transitions in *E. argentinus* crania parallels the evolutionary trends across Traversodontidae suggesting that faunivory in developmentally immature individuals of an herbivorous clade may be plesiomorphic for the clade.

Ontogenetic growth in the crania of *Exaeretodon argentinus* (Synapsida: Cynodontia) captures a dietary shift

Brenen Michael Wynd[1], Fernando Abdala[2,3], and Sterling James Nesbitt[1]

[1]Department of Geosciences, Virginia Tech, Blacksburg, Virginia, U.S.A.

[2]Unidad Ejecutora Lillo, CONICET-Fundación Miguel Lillo, San Miguel de Tucumán, Tucumán, Argentina

3. Evolutionary Studies Institute, University of the Witwatersrand, Johannesburg, South Africa.

Corresponding author:

Brenen Wynd[1]

926 W Campus Dr, Blacksburg, VA, 24061, USA

Email address: bmwynd@vt.edu

Abstract

Ecological differentiation in vertebrates ~~is a common occurrence where~~ ecology shifts with morphology throughout growth. How ecology shifts over a vertebrate's lifetime is often reconstructed in extant species—by combining observational and skeletal data from growth series of the same species—because interactions between organisms and their environment can be observed directly ~~with little inference~~. However, reconstructing shifts using extinct vertebrates is difficult and requires well-sampled growth series, specimens with good preservation, and easily observable skeletal traits associated with the specific ecologies. To reconstruct ecological changes ~~through~~ the growth of a stem-mammal, we describe changes associated with dietary ecology in a growth series of crania of the large-bodied (~2 m in length) and herbivorous form, *Exaeretodon argentinus* (Cynodontia: Traversodontidae) from the Late Triassic, ~~Ischigualasto Formation, San Juan, Argentina. Nearly all specimens were deformed by taphonomic processes, so~~ we reconstructed allometric slope using a generalized linear mixed effects model with distortion as a random effect; ~~previous approaches to reconstruct allometry (ordinary least squares or reduced major axis regression) were not used because they are unable to account for additional variation due to fossilization. Under a mixed effects model,~~ we find that ~~through~~ growth, *E. argentinus* reduced the relative length of the palate, postcanine series, orbits, and basicranium, and expanded the relative length of the temporal region and the height of the zygomatic arch. The allometric relationship between the zygomatic arch and temporal region with the total length of the skull approximate the rate of growth for feeding musculature. Based on a higher allometric slope, the zygoma are growing relatively faster than the temporal

region. The higher rate of change in the zygoma may suggest that smaller individuals had a crushing-dominated feeding style that transitioned into a chewing-dominated feeding style in larger individuals, suggesting a dietary shift from a lower proportion of plant material to a more plant-dominated diet. Dietary differentiation ~~through~~ development is further supported by an increase in sutural complexity and a shift in the orientation of microwear anisotropy between small and large individuals ~~of~~ ~~*E. argentinus*~~. A developmental transition in the feeding ecology ~~of~~ ~~*E. argentinus*~~ is reflective of the reconstructed dietary transition across Gomphodontia, wherein the earliest-diverging species are ~~reconstructed as~~ omnivorous and the well-nested traversodontids are ~~reconstructed as~~ herbivorous. Combining dietary and morphological transitions in *E. argentinus* crania parallels the evolutionary trends across Traversodontidae, suggesting that faunivory in developmentally immature individuals of an herbivorous clade may be plesiomorphic for the clade.

Introduction

Ontogenetic growth characterizes multicellular life, with organisms shifting in absolute size and in the relative size of individual features (Huxley, 1932; Thompson, 1942; Gould, 1968, 1985; Gatsuk et al., 1980; Hochuli, 2001). Patterns of ontogeny have been repeatedly reconstructed in populations and species to estimate underlying constraints on development and evolution (Gould, 1968; Adams, 2000; Sanchez-Villagra, 2010; Goswami et al., 2012; Kolmann et al., 2018; Evans et al., 2019). A mathematical expression of shape change in ontogeny is frequently assessed based on

allometries of numerous individuals from a growth series of the same species, which evaluates the correlations between different features throughout growth (Gould, 1966; Cheverud, 1982; Alexander, 1985; Klingenberg, 1996; Voje et al., 2014; Kilmer & Rodríguez, 2017). ~~Reconstructing~~ allometries in conjunction with ecological observations allows for reconstructions of how organisms interact with their environments and how such interactions shift ~~through~~ growth, ultimately reconstructing the patterns and processes in the evolution of postnatal development.

Ecological shifts during ontogeny are common in vertebrate species, particularly ~~in~~ dietary changes. ~~Examples of ecological changes through ontogeny include shifts from insectivory to herbivory in some extant lizards (Duffield & Bull, 1998), shifts from insectivory to faunivory in the American alligator (Dodson, 1975), increasing amounts of durophagy in the Nile monitor and the hyena (Lonnberg, 1903; Tanner et al., 2010), the shift from altriciality to self-sufficiency in birds and mammals (Herring, 1985; Starck, 1993; To et al., 2021), or from planktivory to piscivory in some fishes (Ross, 1978). However, much of this body of work focuses on extant taxa and direct observations of their ecology and its changes, with fewer reconstructions of ecological change coupled with morphological change.~~ Analyses of morphological change and associated ecological changes in extinct taxa reveal similarly few studies that document such shifts, but is far more difficult because of the incompleteness of the fossil record (Wang et al., 2017).

Species-level allometry has been critical for studies of extinct species, as it is one of the few methods used to estimate patterns of development or even ontogenetic ~~age~~ of extinct species (see also paleohistology; Bailleul, O'Connor & Schweitzer, 2019),

where developmental information is often lost to decay and taphonomic processes (e.g., Sampson, Ryan & Tanke, 1997; Huttenlocker & Abdala, 2015; Hoffman & Rowe, 2018; Griffin & Nesbitt, 2020; Griffin et al., 2020; Hopkins, 2021). Studies that seek to reconstruct ontogeny in extinct species often use measurements that summarize size (e.g., skull length) in comparison with individual measurements (e.g., orbit length) to reconstruct allometric relationships for individual features, with the goals of understanding patterns of growth or to assess if multiple extinct species can be differentiated based on growth curves (e.g., Abdala & Giannini, 2000, 2002; Padian, Horner & De Ricqlès, 2004; Knoll, Padian & de Ricqlès, 2010). However, these studies tend to focus solely on morphology and eclipse ecological interpretations of how shifts in growth may have affected the ecology (i.e., function or diet) of a species.

Previous studies of growth curves and morphological changes in extinct species provide a theoretical backbone ~~to reconstruct~~ how morphological changes in size and shape may influence patterns of ecological change throughout growth. To estimate ecological change through growth in fossils, an element needs to correlate to ecology and have a relatively large sample with variation in size and shape. Furthermore, the fossils should have size-independent characters to confidently identify a growth series as a single species instead of numerous taxa. Non-mammalian cynodonts—a paraphyletic clade of primarily Triassic vertebrates—are an ideal group to evaluate ecological change through ontogeny because their record consists of well-preserved skulls with teeth that are often diagnostic to the species-level (Ruta et al. 2013). Analyses of non-mammalian cynodontian ontogeny using allometry currently represent the earliest diverging epicynodonts and probainognathians (Parrington, 1936; van

Heerden, 1972; Grine & Hahn, 1978; Grine, Hahn & Gow, 1978; Bradu & Grine, 1979; Abdala & Giannini, 2002; Jasinoski, Abdala & Fernandez, 2015; Jasinoski & Abdala, 2017a), with relatively few studies quantitatively reconstructing ontogenetic patterns for taxa that are ~~well~~ nested in the cynodontian subclades (Abdala & Giannini, 2000, 2002; Liu, 2007; Jun, Soares & Reichel, 2008). A clade that is well-suited to estimate correlations between ontogeny and ecology is the Cynognathia (Synapsida; Eucynodontia). Cynognathians include early-diverging faunivorous members (e.g., *Cynognathus crateronotus*) and more well-nested herbivorous taxa (e.g., *Exaeretodon argentinus*). Furthermore, the well nested cynognathian clade Traversodontidae—a clade with faunivorous early diverging members and herbivorous later diverging members—reached relatively large body sizes ~~known~~ and are known from tens of variably sized specimens; thus, allowing a chronicling of change in growth and coordinated shifts in ecology (Goswami et al., 2005; Abdala & Malabarba, 2007; Liu & Abdala, 2014; Kubo, Yamada & Kubo, 2017; Wynd et al., 2017; Hendrickx et al., 2020).

Here we describe the cranial ontogeny of the traversodontid, *Exaeretodon argentinus*, a taxon known from many specimens (n = ~25) from the Ischigualasto Formation of Argentina, and one of the largest bodied South American traversodontids. Large differences in the size range of the *Exaeretodon* growth series (14.9 – 49.6 cm) may suggest that juveniles and adults experienced different trophic interactions, in the form of a dietary shift through growth (see Mittelbach, Osenberg & Leibold, 1988; Schiesari, Werner & Kling, 2009; Start, 2018). ~~We describe the cranial ontogeny based on 16 measurements for 24 individuals, bolstered by previous allometry work (palatal measurements only) that posited *Ischignathus* as a junior subjective synonym of~~

131 ~~*Exaeretodon* (Liu, 2007). Of our sample, 11 specimens were collected from Argentina~~
132 ~~and brought to Harvard in 1965, and 13 are currently housed in Argentina~~. To account
133 for the presence of deformation in a relatively low sample size, we implement a
134 Generalized Linear Mixed Effects model (see Wynd, Uyeda & Nesbitt, 2021), to
135 estimate allometric relationships used to infer ontogenetic change. ~~With this~~
136 ~~reconstruction of ontogeny, we hypothesize a shift in diet from smaller to larger~~
137 ~~individuals~~.
138
139 **Institutional Abbreviations**
140 **MACN**, Museo de Ciencias Naturales “Bernardino Rivadavia”, Buenos Aires, Argentina;
141 **MB.R,** Museum für Naturkunde Berlin, Berlin, Germany; **MCZ VPRA**, The Louis Agassiz
142 Museum of Comparative Zoology, Cambridge, Massachusetts, USA; **MLP**, Museo de
143 La Plata, La Plata, Argentina; **PVL**, Colección de Paleontología de Vertebrados del
144 Instituto Miguel Lillo, San Miguel de Tucumán, Argentina. **PVSJ**, Museo de Ciencias
145 Naturales, Universidad Nacional de San Juan, San Juan, Argentina.
146
147 ## Materials & Methods
148
149 **Specimens**
150 All specimens studied herein were collected from the Ischigualasto Formation in
151 San Juan Province, Argentina. Specimens housed at the MCZ were collected in the
152 1960’s by Alfred Sherwood Romer and his team. Specimens housed at the PVL and
153 MACN were collected by Jose Bonaparte and other Argentinean paleontologists prior to

1994. Since their collection, a 1994 amendment to the Argentine constitution and the subsequent Archaeological and Paleontological Heritage Act of 2003 dictate that fossils belong to the provinces in which they were collected. As such, we recognize the traditional landowners of San Juan, and the Argentinean people to whom these fossils rightfully belong.

Data collection

All data herein were collected by the authors on physical and ~~– due to COVID-19 limiting travel –~~ photographic specimens of *Exaeretodon argentinus* ~~(BMW: MACN, MCZ, PVL, PVSJ; FA: PVL~~), physical measurements were taken using digital calipers for skull length and features and a tailor's measuring tape for skull length of specimens over 300 mm. For digital calipers, we recovered all measurements to the nearest hundredth of a millimeter, and for the tailors tape, we recovered measurements to the nearest tenth of a millimeter. For eight of the studied specimens (see Table 1), we took measurements from photographs using ~~the~~ ImageJ ~~software~~ v. 1.53c (Rasband, 1997; photographs provided by C. Kammerer). We used the 'Set Measurement' function on the scale bar of each photograph, to collect measurements to the nearest hundredth of a millimeter. For all analyses, measurements were rounded to the nearest tenth of a millimeter and log-transformed.

Taphonomic distortion is a critical issue in reconstructing patterns of allometry in extinct animals that often results in measurement omission or estimation (Brown, Arbour & Jackson, 2012; Brown & Vavrek, 2015; Wynd, Uyeda & Nesbitt, 2021). Fortunately, total skull length in *E. argentinus* is typically preserved and not prone to as much

distortion, partly due to regions where many bones contact one another with a relatively large surface area to form resistant structures (e.g., snout vs zygoma). On the other hand, some areas of the skull, particularly regions surrounding the zygomatic arches, where bones are thin and are not supported on all sides by other structures, are more prone to taphonomic deformation; these typically distorted regions result in measurements that deviate from the in-life measurements.

Following Abdala & Giannini (2000), we chose ~~a set of~~ 15 measurements (see Fig. 1 and Table 2), as well as diastema length (DL)—following recent allometric studies of *Thrinaxodon liorhinus* (Jasinoski, Abdala & Fernandez, 2015)—and zygoma width, to incorporate the posterolateral zygomatic shelf to include additional masseteric attachment sites, for a total of 17 measurements (including BSL). We chose these measurements as they can be measured across various cynodonts (and other synapisids) without or with little ambiguity, and they summarize the overall changes in skull shape (Abdala & Giannini, 2000, 2002; Jasinoski, Abdala & Fernandez, 2015; Jasinoski & Abdala, 2017). Furthermore, this set of measurements were all attainable through specimen photographs wherein only dorsal, lateral, and ventral photographs were taken.

For each of the 16 measurements of the skull (see Fig. 1 and Table 2), we scored them as undistorted (0) or distorted (1). Assessing a measure as ‘distorted’ was largely based on deviations from bilateral symmetry (e.g., MCZ VRPA-4469 and PVL 2473), identifying elements that were either misplaced (e.g., misaligned sutures (e.g., MCZ VPRA-4470) and/or there was evidence of twisting or shearing, which was largely ~~localized~~ in the temporal region in *Exaeretodon argentinus* (e.g., MCZ VPRA-4470,

4483, and 4493). We did not collect measurements for features that were entirely missing; for example, both zygomatic arches are missing on MCZ VPRA-4781, and as such, skull width (SW) was not measurable. However, when only one side is missing (e.g., MCZ VPRA-4505), we estimate skull width (SW), as well as other features, based on bilateral symmetry as twice the width from the lateralmost margin of the zygomatic arch to the midpoint of the transverse crest. When only a portion of a feature is missing (e.g., missing premaxilla when measuring muzzle length; MUL), the measurement is taken as is and scored as distorted. In the case of a missing premaxilla (MCZ VPRA-338-58M), we measure basal skull length (BSL), based on the anteriormost extent of the maxilla when the canine or canine alveolus is present, as the anterior extent of the premaxilla is roughly coincident with the anterior extent of an intact maxilla. For features ~~under our criteria as~~ distorted, we take the measurements as is and score those measurements as distorted (1) in our dataset.

~~Contemporary methods to assess ontogenetic age in non-mammalian synapsids~~

~~Estimating direct age in fossil synapsids requires numerous assumptions that are often not available or lack necessary groundtruthing. One such method that has shown promise in numerous lineages is paleohistology (Kolb et al., 2015; Bailleul, O'Connor & Schweitzer, 2019), wherein lines of arrested growth are used to gauge age, based on an assumption of annual cessation in growth due to resource availability, in both extinct and extant lineages. Osteohistology as a metric for skeletochronology can be complicated in lineages in which growth is rapid and continuous (see, *Cynognathus crateronotus*; Botha & Chinsamy, 2000). Although counting lines of arrested growth in~~

histological samples can be used to assess age, much histological work assesses rates and patterns of growth and how histological patterns correlate to size (Botha & Chinsamy, 2000, 2004, 2005; Ray, Botha & Chinsamy, 2004; Botha-Brink, Soares & Martinelli, 2018). By combining histological data with size, relative ages can often be assumed, based on the percent difference in size from the largest individual of the species (Botha & Chinsamy, 2005; Botha-Brink, Soares & Martinelli, 2018). However, using this method in the absence of secondary data assumes that intrapopulation variation in size is relatively small, and that all relatively large bones would belong to developmentally older individuals. Studies that focus on cranial material alone are often unable to utilize osteohistology (but see Botha & Chinsamy, 2004), and are thus limited to using only size as a proxy for age. Fortunately, inferences regarding the appearance of osteological features (e.g., sutural morphology) and their correspondence with body size become possible when either closely related taxa are sampled, data include associated juveniles and adults (Jasinoski & Abdala, 2017b; Hoffman & Rowe, 2018), or clustering methods are used on phylogenetically diverse datasets (Jasinoski, Abdala & Fernandez, 2015; O'Meara & Asher, 2016; Jasinoski & Abdala, 2017a). In the absence of secondary data, the common default is to evaluate the trajectory and patterns of growth via allometric reconstructions (e.g., Cheverud, 1982; Abdala & Giannini, 2000; Blob, 2006; Wynd, Uyeda & Nesbitt, 2021), rather than infer the developmental stage of a single specimen (e.g., juvenile vs adult). In the case of allometry, the statistical parameters that best describe the relationships between specimens (slope and intercept), represent a developmental trajectory, wherein differences between young

and old individuals can be inferred, without ever attributing individual specimens to those developmental categories.

There are currently no models that can estimate an age, exact or relative (e.g., juvenile vs adult), in specimens of *Exaeretodon argentinus*. However, under an allometric framework, we assume that skull length (BSL) is a proxy for age, and that in general, bigger skulls indicate older individuals. Assessing age based on size carries many assumptions with individual specimens, but with allometric models of shape change through growth, we assume that each individual slope and intercept for every feature (e.g., BSL vs MUL) can be used to make inferences about growth. Throughout this manuscript, we avoid the use of relative age terms (e.g., juvenile, subadult, adult) as we cannot identify where in ontogeny these shifts occur, and we cannot confidently assign any region of our allometric models to relative ages. We do not know if our largest specimens reflect the maximum size of *E. argentinus*, and it is clear that we do not have samples of that include the smallest neonates (Hoffman & Rowe, 2018). The smallest individual of *E argentinus* in our sample is 30% the size (BSL; 148.95 mm) of our largest individual BLS; 495.88 mm); because of this, we assume that our specimens, and model interpretations, broadly sample the ontogenetic spectrum from young to old.

Allometric reconstruction

To estimate changes at the ontogenetic level, we reconstruct individual allometries for each of the 16 measurements against basal skull length (BSL; Fig. 1). Ordinary least squares (OLS) regression is commonly used for undistorted

measurements whereas generalized linear mixed models (GLMM) have been explored on datasets that include undistorted and distorted measurements (Wynd, Uyeda & Nesbitt, 2021). The existing sample of *Exaeretodon argentinus* specimens often have distorted features that would lead to dropping those specimens from analysis, which leads to a mean number of available specimens of ~15.5 or 16, rounded. On average, dropping specimens would result in the omission of at least eight specimens per feature, or the estimation of the feature dimensions, which introduces investigator biases into the data. We ~~opt to~~ use a GLMM, which can sufficiently account for additional variation due to distortion ~~in a sample of fossil specimens~~ (Wynd, Uyeda & Nesbitt, 2021). We followed previous methodology and treated the feature of interest as a fixed effect and distortion as a random effect, ~~with no additional fixed effects~~ (Wynd, Uyeda & Nesbitt, 2021). This model assumes random variation due to distortion in the sample and fails to adequately estimate the y-intercept when the distortion is non-random and produces a similar condition in all distorted specimens; however, this caveat does not affect the reconstructed slope (Wynd, Uyeda & Nesbitt, 2021). We indicate a model as having positive or negative allometry when the recovered slope is significantly different from 1.0, which suggests that a feature is isometric and does not change its relative size throughout the lifetime of the organism. We use a p-value < 0.05 as our cutoff for statistical significance, but in cases where the p-value is marginally significant (herein estimated as a p-value $\lesssim$ 0.10, but > 0.05), we report that feature as either reflecting isometry or positive/negative allometry and that the feature would likely be significantly different from isometry with greater sample size. We performed both a linear regression on only undistorted specimens, and a generalized linear mixed model

on the dataset including distorted and undistorted specimens, as an additional method to evaluate model congruence and how model selection (OLS vs GLMM) affects inferences about growth. All analyses were performed in the R statistical environment v. 4.0.2 (~~Team,~~ 2013) and ~~the generalized linear mixed models were performed using the~~ ***lme4*** package v. 1.1.23 (Bates et al., 2007) ~~a commonly used package in fitting and analyzing linear and nonlinear mixed effects models. We report the returned parameters for each of the models (see Table 3) to evaluate the overlap between the two models, linear regression and generalized linear mixed model~~. The ***lme4*** package will return a singular fit warning if one of the effects (fixed or random) has a variance near 0.0—the model is unable to identify variation that exists in the distorted sample but not the undistorted sample or vice versa—indicating that either one of the groups (distorted or undistorted) lacks necessary sample sizes to estimate the variance in the random effect, or that the residuals of the distorted specimens fall within—or very near—the residuals of the undistorted sample. As our random effect is meant to account for taphonomic variation and remove that variation from estimations for the slope, a singular fit is not necessarily a negative result for our model but does require more investigation as to the reason for the lack of variance in the random effect. To evaluate whether there is an impact of body size on the presence of taphonomic deformation, we compare the length of the skull to the total number of distorted features on a single individual, though we only include specimens that can be examined on all sides

To better evaluate how younger individuals of *Exaeretodon argentinus* would have compared morphologically to other cynodonts, we reconstruct hypothetical juveniles of *E. argentinus* based on the ~~outputs~~ of the GLMM. We estimated juvenile

crania with a BSL of 20 and 40 mm (~4% and 8% maximum BSL, respectively) and estimated the size of the zygomas (ZH and ZW) and the temporal region (SW and TEL), as a proxy for general muscle size. We only included slope and y-intercept from the GLMM and did not account for variance around these parameters. We then divided each of these measurements by BSL (20 and 40 mm) in order to estimate the relative size of muscle-bearing cranial features. We then collected the same measurements from a specimen of *Diademodon tetragonus* (MB.R 989), to evaluate whether *E. argentinus* preserves signs of cranial paedomorphosis or has comparable cranial dimensions to a purported omnivore (Botha & Chinsamy, 2000; Ray, Botha & Chinsamy, 2004; Botha, Lee-Thorp & Chinsamy, 2005; Ray, Bandyopadhyay & Bhawal, 2009).

Morphological comparisons

We include brief morphological comparisons between semaphoronts, individual specimens attributed to different growth stages of an ontogeny, to evaluate ontogenetic shifts not readily recognized by linear allometries. Such comparisons primarily focus on sutural morphology and the general morphology of muscle attachment sites.

Dental microwear

To further test whether smaller individuals of *Exaeretodon argentinus* were ecologically similar to larger specimens, we include a qualitative discussion of microwear from the labial surface of an isolated upper left postcanine tooth, attributed to MCZ VPRA-4470. This specimen is cataloged as MCZ VPRA-4470 and is consistent in

size with the postcanine alveoli of the skull of MCZ VPRA-4470 but does not presently fit into any of the open alveoli, which are anteroposteriorly constricted. We molded the labial side of the isolated tooth, using methods outlined by Bestwick et al. (2020); e.g., molds were created with President Jet Regular Body polyvinylsiloxane (Coltène/Whaledent Ltd., Burgess Hill, West Sussex UK) and the first moulds taken from each specimen were discarded to remove any surface material (e.g., dirt, glue parts) and our casts were made on the second molds. Two casts (Smooth-On Smooth-Cast 300 liquid plastic) were made from each mold, for a total of four individual casts of the labial side of the isolated tooth to ensure that the patterns evidenced under the ~~SEM~~ are reflective of the tooth morphology and are not an artifact of the molding and casting process. We used a Hitachi TM3000 ~~tabletop thermionic (tungsten filament source)~~ SEM ~~with polepiece backscattered electron solid-state detector housed in the Virginia Tech Department of Geosciences. Tooth casts were affixed to a stable mount with a combination of clay and double coated carbon conductive tape, to ensure specimen stability and increased conductivity.~~

Systematic paleontology

CYNODONTIA Owen, 1861

TRAVERSODONTIDAE von Huene, 1936, sensu Kammerer et al., 2008

GOMPHODONTOSUCHINAE Watson & Romer, 1956

EXAERETODON Cabrera, 1943

EXAERETODON ARGENTINUS Cabrera, 1943, sensu Liu, 2007

Figs. 1, 4-5

360

361 **Holotype** MLP 43-VII-14-2, incomplete left mandibular ramus.

362 **Diagnostic Characters** We follow previous diagnoses for diagnostic characters, but we
363 exclude mandibular characters as our sample largely lacks associated crania and
364 mandibles. *Exaeretodon* is differentiated from all other traversodontids, except
365 *Siriusgnathus niemeyerorum*, by "[v]ery large traversodontids lacking an internarial bar;
366 upper postcanines with a well-developed posterolabial accessory cusp and extensive
367 shouldering resulting in a separation between a labial lobe and a lingual one (including
368 the occlusal basin); … divergent zygomatic arches; well-developed descending process
369 of the jugal…" (Liu & Abdala 2014, pg. 269). *Exaeretodon* can be differentiated from
370 *Siriusgnathus* by a more distally placed labial accessory cusp of the upper postcanine;
371 rostrum length equal or subequal to the temporal region; a more posteriorly positioned
372 postorbital bar; anteriormost portion of the squamosal reaching the level of the
373 postorbital bar; contact of the squamosal and jugal forming a depression; lambdoidal
374 crest forming a concavity; and a comparatively anteroposteriorly long basicranium
375 (Pavanatto et al., 2018). *Exaeretodon argentinus* can be further differentiated from *E.*
376 *riograndensis* based on the absence of prootic crests, as well as a character pertaining
377 to the mandibular postcanine morphology (Abdala, Barberena & Dornelles, 2002).

378

379 **Referred specimens** MACN: 18125, 18193. MCZ VPRA: 338-58M, 4468, 4470, 4472,
380 4478, 4483, 4486, 4493, 4494, 4505, 4781. PVL: 2056, 2067, 2080, 2082, 2085, 2094,
381 2109, 2473, 2554, 2565. PVSJ 103.

382

Comments The holotype of *Exaeretodon argentinus* was originally described as *Belesodon*? *argentinus* based on an incomplete left ramus of the dentary (Cabrera, 1943). In the same volume, but following the description of *Belesodon*? *argentinus*, the genus *Exaeretodon* was erected with the type species being *E. frenguelli*. However, later work has suggested that *Belesodon*? *argentinus* is actually a specimen of *Exaeretodon frenguelli*, and as such, based on the principle of priority, *E. frenguelli* has been regarded a nomen dubium of *E. argentinus* (sensu Liu, 2007). The type specimen refers only to an incomplete ramus of the dentary and is largely uninformative to the number of *E. argentinus* specimens that either lack mandibles or that have mandibles still bound to the crania by matrix. We extensively use MACN 18125, MCZ VPRA-338-58M, and 4483 as reference specimens, as they consist of complete or nearly complete crania with some or all postcanine teeth in place. Furthermore, they range in size, and retain diagnostic dental characters, strongly suggesting they are of the same species. All of our referred specimens, whose diagnostic features are consistent with MACN 18125, MCZ VPRA-338-58M, and 4483 and lack prootic crests, are attributed to *E. argentinus.*

Results

Allometry

We recover necessary minimum sample sizes of distorted specimens for the GLMM for all measurements, except for length of the upper postcanine series, and maximum width of the zygomatic arch (see Table 3). For the undistorted

measurements, we lack minimum sample sizes for length of the palate, maximum width of the transverse processes of the pterygoids, diameter of the orbit, maximum height of the zygomatic arch, and diastema length. Based on the lack of minimum sample sizes for undistorted specimens, our sample of *Exaeretodon argentinus* crania tend to possess more taphonomic deformation than not. We find no significant relationship between skull length and taphonomic distortion (Fig. 2; α = -0.8529, P (α=1) = 0.837, R^2 = 0.002287), ~~indicating that there is no correlation between distortion and skull size and that the distortion in our dataset is likely randomly distributed across body size~~. Our GLMM is able to estimate allometric relationships with thinner confidence intervals, compared to the OLS, especially when there are more distorted than undistorted measurements (see Fig. 3). For all features we find that the confidence intervals of the GLMM overlap the regression line (See supplemental Figs. S1-S13). Orbit length (OL), upper postcanine length (UP), and basicranial length (BB) were all found to reflect negative allometric relationships under both the OLS and GLMM. Palate length (PAL) and width of the transverse processes (TP) showed an isometric relationship under OLS, but a negative allometric relationship under GLMM, based on marginally significant p-values. Only temporal length (TEL) showed a positive allometric relationship under both models, and zygoma height (ZH) was positive only under GLMM with a marginally significant p-value. All other measurements returned coefficients of allometry that were not significantly different from a slope of 1 and interpreted as isometric. However, those with marginally significant p-values suggest that with greater samples size, they will likely significantly deviate from isometry.

Morphology

The allometric relationships discussed herein offer an insight to how general skull morphology covaries with body size in *Exaeretodon argentinus* (see Fig. 4). A particular challenge in using only allometric relationships between linear measurements, is an assumption that all ontogenetic shifts over a growth series are related to size of a feature, and do not regard the general morphology of the feature (e.g., muscle scars or suture morphology). Herein, we provide a brief description of the observed morphological differences that would not be captured by allometric relationships of linear measurements between small and large individuals of *E. argentinus*.

Snout The snout of *Exaeretodon argentinus* is a complex of tightly sutured bones including the premaxilla, maxilla, nasal, prefrontal, lacrimal and a small contribution from the jugal. The snout often shows minimal deformation, usually in the form of slight twisting or shearing (e.g., MCZ VPRA-4470, 4483, and 4781). Among our sample, several specimens either have some degree of matrix still on the bones or regions of the crania reconstructed with plaster (e.g., MCZ VPRA-4486); these conditions often made it difficult to accurately interpret the bounds of sutural contacts. Therefore, we only report cases where we can confidently interpret sutural morphology (Fig. 5), and we do not report contacts where breaks or matrix make portions of sutural morphology unrecognizable (e.g., Fig. 5C).

The muzzle (MUL) of *E. argentinus* shows an isometric relationship with basal skull length (BSL) throughout ontogeny. When viewing morphological change holistically over the growth series, the muzzle often appears to be relatively shorter in larger

452 individuals, which is likely due to positive allometry of the temporal region (TEL), with a
453 negative allometry of the orbits balancing the anteroposterior growth of the temporal
454 region (Fig. 4). Within the snout, sutural morphology appears to change throughout
455 ontogeny, with larger individuals bearing superficial interdigitation wherein the sutures
456 primarily zig zag to form thin fingers that interlock with one another (Fig. 5D-E).
457 Conversely, smaller individuals tend to have simpler suture morphology, superficially,
458 where bones appear to abut one another without any complex interlocking, clearly
459 represented by the simple sutural contacts between the nasals and surrounding
460 elements (Fig. 5A, B). The contact between the nasals and the frontals, prefrontals,
461 jugals, and lacrimals then shift towards expanded interdigitation in larger individuals,
462 particularly in the regions in which three bones contact one another. The suture
463 between the nasals and the maxillae appears simple across body size; nevertheless,
464 maxillae are only displaced from the nasals in small crania (e.g., MCZ VPRA-4470 and
465 MCZ VPRA-338-58M), which may indicate a more complex sutural contact with internal
466 interdigitation in larger individuals. In smaller individuals, the nasals show an inverse-U
467 shape posteriorly, such that the lateral margins of the nasals extend more posteriorly,
468 resulting in an anterior extension of the frontals fitting between the nasals (Fig. 5B). This
469 relationship appears to change through ontogeny, wherein the nasofrontal contact
470 transitions from a U-shape in smaller individuals to a coronal contact, where the nasals
471 do not expand posteriorly beyond the anterior extent of the frontals.
472
473 **Palate** The palate consists of parts of the premaxilla, maxillae, palatine, and anterior
474 contributions of the pterygoid. The vomer is present in *E. argentinus* but is hidden in

ventral view by the secondary palate. The palatal region shows an overall reduction in the anteroposterior length of the upper postcanine series, as well as an extension of the length of the diastema between the canine and postcanines, consistent with the argument that *E. argentinus*, lost postcanine teeth anteriorly more quickly than they were erupted posteriorly, though at a slower rate than in *E. riograndensis* (Abdala, Barberena & Dornelles, 2002). Although there is discrepancy between the linear regression and the GLMM, the overall length of the palate shows a negative allometry, under the GLMM. As with the snout, the palate is often resistant to deformation, except for some lateral shearing in some specimens (e.g., MCZ VPRA-338-58M, 4468, and 4470). Sutural morphology in the palate appears to remain superficially similar throughout ontogeny. However, few large specimens, with the exception of MCZ VPRA-4483, have fully prepared palates to evaluate ontogenetic changes with confidence. Nevertheless, where visible, the maxilla-palatine, maxilla-premaxilla, and palatine-pterygoid contacts remain simple with no evidence of interdigitation externally.

Temporal region The temporal region consists of the posterior extent of the frontals, the postorbitals, parietals, jugals, squamosals, and quadrates. We exclude contributing elements of the braincase, as the temporal region is interpreted as the temporal fenestra and the surrounding elements, which would have served as attachment sites for the *m. masseter*, *temporalis*, and other feeding related musculature (*m. pseudotemporalis* and *pterygoideus*; see Lautenschlager et al., 2017). The temporal region is the most susceptible to deformation across specimens of *E. argentinus*, including lateral shearing, displacement of elements, or even an entire zygomatic arch

being lost to any combination of breakage or abrasion (e.g., MCZ VPRA-4470, 4486, and 4505). The length of the temporal region and maximum height of the zygoma both show an overall positive allometric pattern (TEL, p=0.0421, significant; ZH, p=0.08026, marginally significant), whereas the overall width of the skull with respect to its total length is isometric. Notably, the rate of expansion (=coefficient of allometry) of the zygoma height (α=1.3084) exceeds the rate of expansion for the length of the temporal region (α=1.1761). Both extinct and extant reconstructions of synapsid cranial musculature reconstruct the temporal fenestra being almost entirely occupied by the *m. temporalis* (Gregory & Adams, 1915; Barghusen, 1973; Hopson, 1994; Sidor, 2001; Kemp, 2005; Lautenschlager et al., 2017). This indicates that the sites for muscle attachment and occupation were both increasing throughout the lifetime of an individual, but that the expansion of the zygoma was outpacing the length of the temporal fenestra (Table 3 and supplemental Fig. S14). Additionally, larger individuals (e.g., MCZ VPRA-4505 and MCZ VPRA-4483) possess a lateral expansion of the zygomatic arch, at its most dorsal and posterior extent, that forms a lateral overhang that increases the total surface-area of the zygomatic arch. However, zygoma width was recovered as isometric (possibly due to sample size); likely due to the anterior extent of the squamosal, which is depressed medially. The depression of the squamosal results in a mediolaterally expanded zygoma in smaller semaphoronts that lack a lateral shelf of the squamosal. By modeling the width of the entire zygoma and not just the width of the jugal or squamosal, the expanded width for small individuals ultimately forces a lower slope and thus an isometric relationship with skull size. All contacts between bones of the temporal region show relatively simple straight suture patterns in smaller individuals

(Fig. 5F), that transition to interdigitating sutures in larger individuals (Fig. 5E). Sutural complexity in larger individuals varies based on orientation, wherein sutures oriented transversely to the skull tend to bear largely sinusoidal morphology with few examples of sutural fingers folding in on one another to form interlocking elements (Fig. 5D). Alternatively, frontally oriented sutures (e.g., postorbital-jugal or frontal-nasal sutures) tend to show more interlocking between elements (Fig. 5D, and E). The connections between these weak to moderately interdigitated sutures tend to be simple, as in the posteroventral border of the postorbital where it articulates with the jugal, laterally (Fig. 5D). Complex interdigitation appears to be absent along the squamosal-jugal contact, which remains simple in both small and large individuals.

Braincase The braincase of *E. argentinus* consists of the basioccipital, opisthotic, basisphenoid, and prootic. The braincase is often well-preserved with lateral shear being most of the deformation observed (e.g., MCZ VPRA-4493). Like the snout, the braincase is a region of many tightly sutured bones that produce a relatively resistant structure to deformation. The anteroposterior length of the braincase (BB) shows a negative allometric trend, which is generally consistent with the notion that regions of the skull that house the brain and sensory organs often show negative allometric relationships in vertebrates (Howland, Merola & Basarab, 2004). In contrast, the occipital plate width (OW) has an overall isometric pattern, which is perhaps related to the fact that the measurement (or variable) is reflecting the braincase width but also the enlargement of the splanchnocranial apparatus. Isometry in the width of the skull would indicate that although the braincase is growing at a constant rate mediolaterally (OW)—

and potentially covarying with other cranial features that correspond with jaw placement (e.g., width of transverse processes; TP)—it is getting relatively shorter anteroposteriorly (BB) through growth. As with the palate, many larger specimens of *E. argentinus* have ventrally underprepared braincases making accurate reconstructions of suture morphology difficult to assess. What is available suggests overall similar sutural patterns as elsewhere in the skull, wherein braincases of smaller individuals (e.g., MCZ VPRA-4781) bear simple sutures with little to no interdigitation both ventrally and on the lateral wall. Few ventral sutures are evident in larger skulls, with the exception of the opisthotic-squamosal contact, which is consistently simple and lacks any evidence of interdigitation. In contrast, the parietal-squamosal contact bears interlocking fingers, similar in morphology for those described for the frontal-nasal suture.

Dental microwear

Qualitative assessments of dental microwear texture reveal patterns of anisotropy (parallel scratch marks or ridges) and low complexity on the labial margin of the upper left postcanine attributed to a small individual of *Exaeretodon argentinus* (see Fig. 6A-C). However, wear facets (Fig. 6D), appear to have little anisotropy and are largely dominated by some degree of pitting and irregular abraded surfaces. The only other account of dental microwear texture in *E. argentinus* focused on what were considered to be adult specimens (PVSJ 707: BSL~29 cm; PVSJ 1091; BSL~30 cm; Kubo, Yamada & Kubo, 2017). Microwear in purported adult specimens revealed primarily anisotropic patterns, wherein the majority of scratches are oriented within 20° of the anteroposterior orientation of the tooth (Kubo, Yamada & Kubo, 2017). The

patterns evidenced herein appear to be oriented more along the dorsoventral axis of the tooth and are thus ~90° displaced from scratches on teeth of larger individuals. Microwear displacement between small and large individuals may reflect masticatory and/or dietary differentiation between small and large individuals.

Discussion

Osteological shifts through ontogeny ~~discerned by mixed effects models~~

~~Discerning age and overall developmental patterns from the fossil record using only size is a difficult task that requires multiple lines of evidence to best ensure that a growth curve represents only one taxon (Sampson, Ryan & Tanke, 1997; Abdala & Giannini, 2000; Griffin & Nesbitt, 2016; Hone, Farke & Wedel, 2016; Griffin et al., 2021). We assess morphological change by modeling changes in size through allometry, using regressions to hypothesize how a species may have developmentally changed through age. By combining such quantitative change through regressions with qualitative changes in external morphology, we can more appropriately estimate ontogenetic trajectories in extinct taxa~~. There are striking morphological differences in *Exaeretodon argentinus* from small (14.9 cm long) to large skulls (49.6 cm long). More than half (nine of 16) of cranial features measured for *Exaeretodon argentinus* are isometric with respect to differences in basal skull length (BSL; that we interpret as a proxy of age). Most notable deviations from isometry are the anteroposterior expansion of the temporal region (TEL), and the overall reduction of the braincase (BB), orbit size (OL), and the palate (PAL) and associated dentition (UP). Additionally, ~~under the GLMM,~~ the

width of the transverse process of the pterygoid (TP; negative allometry), and the height of the zygomatic arch (ZH; positive allometry) are marginally significant. The lateral face of the transverse process is in contact with the medial surface of the mandible (Crompton, 1995) and the reduction in width of the transverse processes (TP) likely reflects a mediolateral expansion of the temporal opening, and a relatively more central position of the mandible in the opening, in connection with a more developed occlusal musculature ~~(Fig. 4B).~~ A similar trend, although more extreme, was reported for the epicynodont *Galesaurus*, in which the mandible of younger individuals was laterally located near the zygomatic arch, indicating widely separated transverse processes (Jasinoski and Abdala, 2017a).

Myological shifts through ontogeny interpreted through allometric relationships

Evaluating changes in musculature based on allometric coefficients often requires an assumption that measurements on a dry skull (surface area of attachment sites) are roughly proportional to muscle dimensions measured from a dissection. A dry-skull inference will always be an underestimate of muscle size, as the smallest a muscle can ever be is the osteological area of attachment. As it stands, the dry skull inference may not be useful or accurate when comparing multiple species to one another, even those from the same clade (Law & Mehta, 2019; Bates et al., 2021). Surprisingly, given an ontogenetic dataset, size and covariation between muscles and their attachment sites, or even between different attachment sites, may also not be reflective of the musculature or functional estimates derived from musculature (CJL pers comm; Law & Mehta, 2019). Critically, using only the measurement of an attachment site in an

individual mammal, or a growth series of a species of mammals, is not a reliable method to interpret function or ecology (Hutchinson, 2012; Toro-Ibacache, Zapata Muñoz & O'higgins, 2015; Bates et al., 2021; Broyde et al., 2021). As such, we looked to combining changes in allometric parameters (slope and intercept), to evaluate the rate of change between features, with overall morphology and how their correlations may be reflective of function and ecology.

The *m. masseter* and *temporalis* are often discussed in their roles in chewing and crushing, respectively. The *m. masseter* anchors onto the zygomatic arch on the skull, and, the masseteric fossa on the coronoid process of the dentary (Crompton, 1963). The bounds for the masseter in *E. argentinus* are estimated herein based on the zygoma height (ZH) and width (ZW). The *m. temporalis* anchors to the sagittal crest and occupies the available space in the temporal fenestra, and its bounds are estimated herein based on the skull width (SW) and length of the temporal region (TEL). The width of the skull (SW) and width of the zygoma (ZW) have overall isometric relationships, indicating a relatively constant relationship as skull length increases. Conversely, the length of the temporal region (TEL), and height of the zygoma (ZW) have positive allometric relationships, indicating a faster rate of growth in comparison to skull length. The rate of change in the *m. masseter* (ZH; α= 1.31) outpaces that of the *m. temporalis* (TEL; α= 1.18), suggesting that the *m. masseter* could be growing at a faster rate than the *m. temporalis*. To further evaluate this relationship, the *masseter* also originates in smaller individuals of *E. argentinus* at a relatively smaller size (ZH; β= -1.33) than the *m. temporalis* (TEL; β= -0.83). Furthermore, the presence of highly interdigitated

635 sutures between the frontals and the nasals in larger individuals may reflect a structural
636 counterbalance to the strain imposed by the *m. masseter* (Herring & Teng, 2000).
637 This would then suggest that *Exaeretodon argentinus* shifted their masticatory
638 use through growth, with a *m. temporalis*-driven bite in juveniles, followed later by a *m.*
639 *masseter*-driven bite in older individuals. Changes in the relative size of the feeding
640 musculature is likely correlated with diet, such that *E. argentinus* may have transitioned
641 from a faunivorous juvenile stage to an herbivorous adult stage, as is seen in Australian
642 skinks (e.g., Duffield & Bull, 1998). Further investigation into stable isotope
643 geochemistry (e.g., isotopic carbon/nitrogen as proxies for trophic position) and long-
644 bone histology (e.g., lines of arrested growth and vasculature as proxies for continuous
645 or periodic growth) will be imperative to support this hypothesis in future studies.
646 Presently, we explore observations of sutural complexity and dental microwear between
647 small and large individuals of *E. argentinus* to evaluate whether additional systems
648 support dietary differentiation through growth.
649
650 **Changes in suture complexity over the *Exaeretodon* growth series**
651 Qualitative differences between semaphoronts includes smaller individuals
652 bearing relatively simple non-interdigitated sutures surrounding the maxilla, suggesting
653 that they would not have been able to exert much force in mastication (e.g., mouse and
654 theropods: Byron et al., 2004; Rayfield, 2005). Larger individuals bear more
655 interdigitating sutures—notched contacts where fingers of each bone overlap one
656 another to increase surface area of contact—throughout the snout and braincase,
657 reflecting enhanced structural integrity for increased and sustained force exertion during

658 mastication, and the ability to process harder food objects (Monteiro & Lessa, 2000;
659 Byron et al., 2004; Byron, 2009). The snout and braincase are regions where multiple
660 bones contact one another resulting in highly sutured areas. Increases in complexity
661 (i.e., interdigitation vs simple contacts) through growth reflects an increase in surface
662 area of the sutural contacts, which suggests that the snout and braincase would be
663 more resistant to stresses (such as masticatory), in older individuals (White et al.,
664 2020). This is further supported by the lack of deformation (e.g., element displacement)
665 in larger individuals in those regions. The process of increasing sutural complexity does
666 not include the maxilla, as it retains a simple suture throughout this growth series, and is
667 offset considerably in smaller individuals (e.g., MCZ VPRA-338-58M), as opposed to the
668 condition in some larger individuals (e.g., MCZ VPRA-4483), where maxillary
669 displacement from the nasals is minimal. A difference in degree of displacement
670 between small and large individuals may suggest that the snouts are somewhat resilient
671 to forces and stresses that would come from mastication (Jasinoski, Rayfield &
672 Chinsamy, 2010; Maloul et al., 2014) and thus it is key to evaluate and reconstruct
673 developmental patterns for the muscles that dominate feeding in tetrapods, the *m.*
674 *masseter and temporalis*. Jasinoski et al. (2015) also reported an increased complexity
675 of particular sutures (i.e., nasal-frontal) towards adulthood in *Thrinaxodon*.
676
677 **Microwear texture supports heterogeneity in diet through growth**
678 To further evaluate ecological differentiation through growth in *Exaeretodon*
679 *argentinus*, we evaluate microwear texture on the labial margin of an isolated upper left
680 postcanine tooth attributed to one of the smaller individuals in our sample (MCZ VPRA-

4470; BSL=16.7 cm). Anisotropy, parallel lines, is the primary texture on the labial surface of the tooth; however, such lines are sparse and are only weakly scraped. These patterns do not reflect scratching or gouging from occlusion during mastication, but instead reflect abrasion as differing food items would have interacted with the labial margin of a tooth throughout mastication (Calandra & Merceron, 2016). Patterns of anisotropy have largely been present in amniotes that have primarily faunivorous diets (DeSantis, 2016; Bestwick et al., 2020). Anisotropy is also recovered as the predominant texture in larger individuals of *E. argentinus* (Kubo, Yamada & Kubo, 2017), but are instead displaced 90° in the tooth of the smaller individual (MCZ VPRA-4470). The microwear of larger individuals has been interpreted to reflect propalinal movement of the jaw, which can be interpreted as an *m. masseter* driven mastication (Kubo, Yamada & Kubo, 2017). Herein, we find that the anisotropic patterns of a small individual (MCZ VPRA-4470) are oriented apicobasally, perpendicular to the orientation of scratches evidenced in larger individuals of *E. argentinus* (Kubo, Yamada & Kubo, 2017). If the patterns of anisotropy in MCZ VPRA-4470 are similarly reflective of jaw motion, mastication would be primarily orthal, suggesting an *m. temporalis* driven bite (see Grossnickle et al. 2021 and references therein), *contra* to the inferred palinal movements in larger *Exaeretodon* (Kubo, Yamada & Kubo, 2017). Interpreting ecological differentiation based on microwear alone assumes all dental modifications are feeding-related but finding consistent patterns in the ontogeny of masticatory muscle sizes and sutural complexity all together support younger individuals of *E. argentinus* having a dietary ecology distinct from older conspecifics.

704 **Dietary differentiation through ontogeny in *Exaeretodon argentinus***

705 Our hypothesis that *Exaeretodon argentinus* went through a dietary shift through
706 growth is supported by changes in cranial structures and proportions, microwear, and
707 sutural pattern changes. This hypothesis is supported by 1) relative expansion of the
708 areas and openings for the attachment of the *m. masseter* and *temporalis*; 2) increases
709 in sutural complexity in the snout and the cranium; and 3) displacement in microwear
710 anisotropy from small to large individuals. Taken together, these concurrent changes
711 suggest ecological differentiation with growth, related to differentiation in feeding
712 ecology. Current assumptions of herbivory in species of *Exaeretodon* (Martínez et al.,
713 2012; Francischini, Dentzien-Dias & Schultz, 2018; Melo et al., 2019) would then
714 suggest that younger individuals would have been ecologically distinct, and were likely
715 more faunivorous than older contemporaries, an ecological strategy known in Australian
716 skinks, bearded dragons, spiny tailed-iguanas, and numerous omnivorous lizards
717 (Duffield & Bull, 1998; Cooper & Vitt, 2002; Wotherspoon & Burgin, 2016). Because we
718 cannot estimate the complete growth curve of the taxon, we can't pinpoint when this
719 transition may have occurred, but identify that younger (smaller) individuals are
720 morphologically and functionally distinct from older (larger) individuals.

721

722 ***Exaeretodon* ontogeny suggests developmental constraint within traversodontids**

723 The proposed changes in dietary ecology through growth in *Exaeretodon*
724 *argentinus* parallels macroevolutionary patterns of dietary change across Cynognathia.
725 The earliest diverging cynognathians are reconstructed as primarily carnivorous, to
726 purported omnivorous gomphodontians, and to the well-nested herbivorous

traversodontids. Parallels between the ontogeny of *E. argentinus* and the evolution of diet across Cynognathia may indicate some degree of constraint on the broader clade. The allometric patterns of *Exaeretodon argentinus* are consistent with those of *Massetognathus pascuali*. Albeit these taxa differ in the magnitude of estimated slopes (e.g., rates of change) and significance of those slopes, but conserved patterns of positive and negative allometry suggest a similar growth pattern between these well-nested traversodontids (~~Table 4).~~ Furthermore, many of these features are also consistent with patterns of *Diademodon tetragonus* (Bradu & Grine, 1979; Grine & Hahn, 1978; Grine, Hahn & Gow, 1978), one of the earliest diverging cynognathians, potentially indicating that cynognathians possess a constrained growth pattern distinct from non-cynognathian eucynodonts. Recovering a consistent allometric pattern across presently sampled gomphodonts—the last common ancestor of *Diademodon tetragonus* and *Exaeretodon argentinus* and all of its descendants (Sues & Hopson, 2010)—suggests that cynognathian evolution may be the result of developmental canalization. If this is the case, we would expect that a small individual of *E. argentinus* would have a skull with features whose relative sizes are reflective of early diverging cynognathians. Based on extrapolations of the allometric coefficients presented here, we recover a young individual (estimated BSL=40 cm; ~10% maximum: BSL=20 cm; 5% maximum) that is unlike undistorted representatives of *Diademodon tetragonus* (e.g., MB.R 989). However, these hypothetical young individuals had relatively smaller temporal regions (average TEL~66% and SW~70%) and much reduced zygomatic arches (average ZH~34% and ZW~58%), compared to a large *D. tetragonus* individual (Table 5). Given the proposed faunivorous lifestyle of *D. tetragonus*, these relationships propose neonate

individuals of *E. argentinus* with potentially faunivorous tendencies, based on the relative contribution of the regions anchoring the *m. temporalis* (TEL and SW), compared to the relatively smaller contributions of the regions anchoring the *m. masseter* (ZH and ZW). Such a transition from faunivory to herbivory in *Exaeretodon argentinus* would thus mirror the evolution of diet in traversodontids (Grine, 1978; Botha, Lee-Thorp & Chinsamy, 2005; Goswami et al., 2005; Kubo, Yamada & Kubo, 2017), indicating a degree of phylogenetic retention along with developmental constraints reflective of the broader clade.

Until recently, the Traversodontidae has been considered a clade of likely exclusive herbivores, with the discovery of *Etjoia dentitransitus* as the earliest-diverging traversodontid suggesting faunivory as a possible plesiomorphic condition for the clade (Hendrickx et al., 2020). By including young *Exaeretodon* as an additional faunivorous traversodontid, it would follow that faunivory was potentially present throughout Traversodontidae in earlier ontogenetic stages and is not homoplastic in gomphodontosuchines. Additional analyses of ontogeny in traversodontids will be critical to assess if faunivory in young individuals is consistent across the entire clade, or if *Exaeretodon* represents a relatively slow development, in which masticatory modification occurs postnatally. Regardless, the occurrence of faunivory amongst well-nested herbivores indicates a need to re-evaluate the evolution of herbivory across the tree of life, and how differing developmental strategies are associated with ecological differentiation.

Acknowledgements

The authors thank Stephanie J. Pierce, Jessica Cundiff, and Christina Byrd at the Museum of Comparative Zoology, Harvard University for allowing access to specimens. They acknowledge that all *Exaeretodon* from the Harvard Museum of Comparative Zoology were collected from Argentina in the 1960's by Alfred Sherwood Romer and colleagues, and rightfully belong to the province of San Juan, Argentina, following amendments to the Argentine constitution in 1994, and the subsequent Archaeological and Paleontological Heritage Act in 2003. They thank Christian Kammerer, for providing photographs of various cynodontians that made this work possible, given travel restrictions due to COVID-19. They thank Chris Law for discussion of dry skull muscle estimation and providing data to run additional tests. They also thank Josef Uyeda, Michelle Stocker, Christopher Griffin, Casey Holliday, and the Virginia Tech Paleobiology group for helpful discussion.

References

Abdala F, Barberena MC, Dornelles J. 2002. A new species of the traversodontid cynodont *Exaeretodon* from the Santa Maria Formation (Middle/Late Triassic) of southern Brazil. *Journal of Vertebrate Paleontology* 22:313–325.

Abdala F, Giannini NP. 2000. Gomphodont cynodonts of the Chañares Formation: the analysis of an ontogenetic sequence. *Journal of Vertebrate Paleontology* 20:501–506.

Abdala F, Giannini NP. 2002. Chiniquodontid cynodonts: Systematic and morphometric considerations. *Palaeontology* 45:1151–1170. DOI: 10.1111/1475-4983.00280.

Abdala F, Malabarba MC. 2007. Enamel microstructure in *Exaeretodon*, a Late Triassic

796 south american traversodontid (Therapsida: Cynodontia). *Rev. Bras. Paleontolog*
797 10:71–78.
798 Adams RA. 2000. Wing ontogeny, shifting niche dimensions, and adaptive landscapes.
799 *Ontogeny, functional ecology, and evolution of bats (RA Adams and SC Pedersen,*
800 *eds.). Cambridge University Press, Cambridge*:275–315.
801 Alexander RM. 1985. Body support, scaling, and allometry. *Functional vertebrate*
802 *morphology* 38:57.
803 Bailleul AM, O'Connor J, Schweitzer MH. 2019. Dinosaur paleohistology: review, trends
804 and new avenues of investigation. *PeerJ* 7:e7764.
805 Barghusen HR. 1973. The adductor jaw musculature of *Dimetrodon* (Reptilia,
806 Pelycosauria). *Journal of Paleontology*:823–834.
807 Bates D, Sarkar D, Bates MD, Matrix L. 2007. The lme4 package. *R package version*
808 2:74.
809 Bates KT, Wang L, Dempsey M, Broyde S, Fagan MJ, Cox PG. 2021. Back to the
810 bones: do muscle area assessment techniques predict functional evolution across
811 a macroevolutionary radiation? *Journal of the Royal Society Interface* 18:20210324.
812 Bestwick J, Unwin DM, Butler RJ, Purnell MA. 2020. Dietary diversity and evolution of
813 the earliest flying vertebrates revealed by dental microwear texture analysis. *Nature*
814 *communications* 11:1–9.
815 Blob RW. 2006. Scaling of the hind limb skeleton in cynognathian cynodonts:
816 implications for ontogeny and the evolution of mammalian endothermy. *Amniote*
817 *paleobiology: perspectives on the evolution of mammals, birds, and reptiles.*
818 *Chicago: University of Chicago Press. p*:410–428.

819 Botha-Brink J, Soares MB, Martinelli AG. 2018. Osteohistology of Late Triassic
820 prozostrodontian cynodonts from Brazil. *PeerJ* 6:e5029.
821 Botha J, Chinsamy A. 2000. Growth patterns deduced from the bone histology of the
822 cynodonts *Diademodon* and *Cynognathus*. *Journal of Vertebrate Paleontology*
823 20:705–711.
824 Botha J, Chinsamy A. 2004. Growth and life habits of the Triassic cynodont
825 *Trirachodon*, inferred from bone histology.
826 Botha J, Chinsamy A. 2005. Growth patterns of *Thrinaxodon liorhinus*, a
827 non-mammalian cynodont from the Lower Triassic of South Africa. *Palaeontology*
828 48:385–394.
829 Botha J, Lee-Thorp J, Chinsamy A. 2005. The palaeoecology of the non-mammalian
830 cynodonts *Diademodon* and *Cynognathus* from the Karoo Basin of South Africa,
831 using stable light isotope analysis. *Palaeogeography, Palaeoclimatology,*
832 *Palaeoecology* 223:303–316.
833 Bradu D. Grine FE. 1979. Multivariate analysis of diademodontine crania from South
834 Africa and Zambia. *South African Journal of Science* 75:441–448.
835 Brown CM, Arbour JH, Jackson DA. 2012. Testing of the effect of missing data
836 estimation and distribution in morphometric multivariate data analyses. *Systematic*
837 *biology* 61:941–954.
838 Brown CM, Vavrek MJ. 2015. Small sample sizes in the study of ontogenetic allometry;
839 implications for palaeobiology. *PeerJ* 3:e818.
840 Broyde S, Dempsey M, Wang L, Cox PG, Fagan M, Bates KT. 2021. Evolutionary
841 biomechanics: hard tissues and soft evidence? *Proceedings of the Royal Society B*

288:20202809.

Byron CD. 2009. Cranial suture morphology and its relationship to diet in *Cebus*. *Journal of human evolution* 57:649–655.

Byron CD, Borke J, Pashley D, Wingard CJ, Hamrick M. 2004. Effects of increased muscle mass on mouse sagittal suture morphology and mechanics. *The Anatomical Record Part A: Discoveries in Molecular, Cellular, and Evolutionary Biology: An Official Publication of the American Association of Anatomists* 279:676–684.

Cabrera A. 1943. *El primer hallazgo de terápsidos en la Argentina*. Instituto del Museo de la Universidad Nacional de La Plata.

Calandra I, Merceron G. 2016. Dental microwear texture analysis in mammalian ecology. *Mammal Review* 46:215–228.

Cheverud JM. 1982. Relationships among ontogenetic, static, and evolutionary allometry. *American Journal of Physical Anthropology* 59:139–149.

Crompton AW. 1963. The evolution of the mammalian jaw. *Evolution*:431–439.

Crompton AW. 1995. Masticatory function in nonmammalian cynodonts and early mammals. *Functional morphology in vertebrate paleontology*:55–75.

DeSantis LRG. 2016. Dental microwear textures: reconstructing diets of fossil mammals. *Surface Topography: Metrology and Properties* 4:23002.

Dodson P. 1975. Functional and ecological significance of relative growth in *Alligator*. *Journal of Zoology* 175:315–355. DOI: 10.1111/j.1469-7998.1975.tb01405.x.

Duffield GA, Bull CM. 1998. Seasonal and ontogenetic changes in the diet of the Australian skink *Egernia stokesii*. *Herpetologica*:414–419.

865 Evans KM, Bernt MJ, Kolmann MA, Ford KL, Albert JS. 2019. Why the long face? Static
866 allometry in the sexually dimorphic phenotypes of Neotropical electric fishes.
867 *Zoological Journal of the Linnean Society* 186:633–649.
868 Francischini H, Dentzien-Dias P, Schultz CL. 2018. A fresh look at ancient dungs: the
869 Brazilian Triassic coprolites revisited. *Lethaia* 51:389–405.
870 Gatsuk LE, Smirnova O V, Vorontzova LI, Zaugolnova LB, Zhukova LA. 1980. Age
871 states of plants of various growth forms: a review. *The Journal of Ecology*:675–696.
872 Goswami A, Flynn JJ, Ranivoharimanana L, Wyss AR. 2005. Dental microwear in
873 Triassic amniotes: implications for paleoecology and masticatory mechanics.
874 *Journal of Vertebrate Paleontology* 25:320–329.
875 Goswami A, Polly PD, Mock OB, Sánchez-Villagra MR. 2012. Shape, variance and
876 integration during craniogenesis: contrasting marsupial and placental mammals.
877 *Journal of evolutionary biology* 25:862–872.
878 Gould SJ. 1966. Allometry and size in ontogeny and phylogeny. *Biological reviews of*
879 *the Cambridge Philosophical Society* 41:587–640. DOI: 10.1111/j.1469-
880 185x.1966.tb01624.x.
881 Gould SJ. 1968. Ontogeny and the explanation of form: an allometric analysis. *Memoir*
882 *(The Paleontological Society)*:81–98.
883 Gould SJ. 1985. *Ontogeny and phylogeny*. Harvard University Press.
884 Gregory WK, Adams LA. 1915. The temporal fossae of vertebrates in relation to the jaw
885 muscles. *Science*:763–765.
886 Griffin CT, Nesbitt SJ. 2016. The femoral ontogeny and long bone histology of the
887 Middle Triassic (? late Anisian) dinosauriform *Asilisaurus kongwe* and implications

for the growth of early dinosaurs. *Journal of Vertebrate Paleontology* 36:e1111224.

Griffin CT, Nesbitt SJ. 2020. Does the maximum body size of theropods increase across the Triassic–Jurassic boundary? Integrating ontogeny, phylogeny, and body size. *The Anatomical Record* 303:1158–1169.

Griffin CT, Stocker MR, Colleary C, Stefanic CM, Lessner EJ, Riegler M, Formoso K, Koeller K, Nesbitt SJ. 2021. Assessing ontogenetic maturity in extinct saurian reptiles. *Biological Reviews* 96:470–525.

Grine FE. 1978. Postcanine dental structure in the mammal-like reptile *Diademodon* (Therapsida; Cynodontia). In: *Proc Electron Microsc Soc S Afr*. 123–124.

Grine FE, Hahn BD. 1978. Allometric growth in the Diademodontinae (Reptilia; Therapsida); a preliminary report.

Grine FE, Hahn BD, Gow CE. 1978. Aspects of relative growth and variability in *Diademodon* (Reptilia: Therapsida). *South African Journal of Science* 74:50.

Grossnickle DM, Weaver LN, Jäger KR, Schultz JA. 2021. The evolution of anteriorly directed molar occlusion in mammals. *Zoological Journal of the Linnean Society*: doi.org/10.1093/zoolinnean/zlab039

Hendrickx C, Gaetano LC, Choiniere JN, Mocke H, Abdala F. 2020. A new traversodontid cynodont with a peculiar postcanine dentition from the Middle/Late Triassic of Namibia and dental evolution in basal gomphodonts. *Journal of Systematic Palaeontology* 18:1669–1706.

Herring SW. 1985. The ontogeny of mammalian mastication. *American Zoologist* 25:339–350.

Herring SW, Teng S. 2000. Strain in the braincase and its sutures during function.

American Journal of Physical Anthropology: The Official Publication of the American Association of Physical Anthropologists 112:575–593.

Hochuli DF. 2001. Insect herbivory and ontogeny: how do growth and development influence feeding behaviour, morphology and host use? *Austral Ecology* 26:563–570.

Hoffman EA, Rowe TB. 2018. Jurassic stem-mammal perinates and the origin of mammalian reproduction and growth. *Nature* 561:104–108.

Hone DWE, Farke AA, Wedel MJ. 2016. Ontogeny and the fossil record: what, if anything, is an adult dinosaur? *Biology Letters* 12:20150947.

Hopkins MJ. 2021. Ontogeny of the trilobite *Elrathia kingii* (Meek) and comparison of growth rates between *Elrathia kingii* and *Aulacopleura koninckii* (Barrande). *Papers in Palaeontology* 7:985–1002.

Hopson JA. 1994. Synapsid evolution and the radiation of non-eutherian mammals. *Short Courses in Paleontology* 7:190–219.

Howland HC, Merola S, Basarab JR. 2004. The allometry and scaling of the size of vertebrate eyes. *Vision research* 44:2043–2065.

von Huene F. 1935. *Die fossilen Reptilien des südamerikanischen Gondwanalandes an der Zeitenwende: Ergebnisse d. Sauriergrabungen in Südbrasilien 1928/29*. Beck.

Hutchinson JR. 2012. On the inference of function from structure using biomechanical modelling and simulation of extinct organisms. *Biology letters* 8:115–118.

Huttenlocker AK, Abdala F. 2015. Revision of the first therocephalian, *Theriognathus* Owen (Therapsida: Whaitsiidae), and implications for cranial ontogeny and allometry in nonmammaliaform eutheriodonts. *Journal of Paleontology* 89:645–664.

934 Jasinoski SC, Abdala F. 2017a. Cranial Ontogeny of the Early Triassic Basal Cynodont
935 *Galesaurus planiceps*. *Anatomical Record* 300:353–381. DOI: 10.1002/ar.23473.
936 Jasinoski SC, Abdala F. 2017b. Aggregations and parental care in the Early Triassic
937 basal cynodonts *Galesaurus planiceps* and *Thrinaxodon liorhinus*. *PeerJ* 5:e2875.
938 Jasinoski SC, Abdala F, Fernandez V. 2015. Ontogeny of the Early Triassic Cynodont
939 *Thrinaxodon liorhinus* (Therapsida): Cranial Morphology. *Anatomical Record*
940 298:1440–1464. DOI: 10.1002/ar.23116.
941 Jasinoski SC, Rayfield EJ, Chinsamy A. 2010. Functional implications of dicynodont
942 cranial suture morphology. *Journal of Morphology* 271:705–728.
943 Kammerer CF, Flynn JJ, Ranivoharimanana L, Wyss AR. 2008. New material of
944 *Menadon besairiei* (Cynodontia: Traversodontidae) from the Triassic of
945 Madagascar. *Journal of Vertebrate Paleontology* 28:445–462.
946 Kemp TS. 2005. *The origin and evolution of mammals*. Oxford University Press on
947 Demand.
948 Kilmer JT, Rodríguez RL. 2017. Ordinary least squares regression is indicated for
949 studies of allometry. *Journal of evolutionary biology* 30:4–12.
950 Klingenberg CP. 1996. Multivariate Allometry. *Advances in Morphometrics*:23–49. DOI:
951 10.1007/978-1-4757-9083-2_3.
952 Knoll F, Padian K, de Ricqlès A. 2010. Ontogenetic change and adult body size of the
953 early ornithischian dinosaur *Lesothosaurus diagnosticus*: implications for basal
954 ornithischian taxonomy. *Gondwana Research* 17:171–179.
955 Kolb C, Scheyer TM, Veitschegger K, Forasiepi AM, Amson E, Van der Geer AAE, Van
956 den Hoek Ostende LW, Hayashi S, Sánchez-Villagra MR. 2015. Mammalian bone

957 palaeohistology: a survey and new data with emphasis on island forms. *PeerJ*
958 3:e1358.
959 Kolmann MA, Huie JM, Evans K, Summers AP. 2018. Specialized specialists and the
960 narrow niche fallacy: a tale of scale-feeding fishes. *Royal Society open science*
961 5:171581.
962 Kubo T, Yamada E, Kubo MO. 2017. Masticatory jaw movement of *Exaeretodon*
963 *argentinus* (Therapsida: Cynodontia) inferred from its dental microwear. *PloS one*
964 12:e0188023.
965 Lautenschlager S, Gill P, Luo Z, Fagan MJ, Rayfield EJ. 2017. Morphological evolution
966 of the mammalian jaw adductor complex. *Biological Reviews* 92:1910–1940.
967 Law CJ, Mehta RS. 2019. Dry versus wet and gross: Comparisons between the dry
968 skull method and gross dissection in estimations of jaw muscle cross-sectional area
969 and bite forces in sea otters. *Journal of morphology* 280:1706–1713.
970 Liu J. 2007. The taxonomy of the traversodontid cynodonts *Exaeretodon* and
971 *Ischignathus*. *Revista Brasileira de Paleontologia* 10:133–136.
972 Liu J, Soares MB, Reichel M. 2008. *Massetognathus* (Cynodontia, Traversodontidae)
973 from the Santa Maria Formation of Brazil. *Revista brasileira de paleontologia. Vol. 11, n.*
974 *1 (jan./abr. 2008), p. 27-36*.
975 Liu J, Abdala F. 2014. Phylogeny and taxonomy of the Traversodontidae. In: *Early*
976 *evolutionary history of the Synapsida*. Springer, 255–279.
977 Lonnberg E. 1903. On the adaptations to a molluscivorous diet in *Varanus niloticus*.
978 *Arkiv for Zoologi* 1:67–83.
979 Maloul A, Fialkov J, Wagner D, Whyne CM. 2014. Characterization of craniofacial

sutures using the finite element method. *Journal of biomechanics* 47:245–252.

Martínez RN, Apaldetti C, Alcober OA, Colombi CE, Sereno PC, Fernandez E, Malnis PS, Correa GA, Abelin D. 2012. Vertebrate succession in the ischigualasto formation. *Journal of Vertebrate Paleontology* 32:10–30. DOI: 10.1080/02724634.2013.818546.

Melo TP, Ribeiro AM, Martinelli AG, Soares MB. 2019. Early evidence of molariform hypsodonty in a Triassic stem-mammal. *Nature communications* 10:1–8.

Mittelbach GG, Osenberg CW, Leibold MA. 1988. Trophic relations and ontogenetic niche shifts in aquatic ecosystems. In: *Size-structured populations*. Springer, 219–235.

Monteiro LR, Lessa LG. 2000. Comparative analysis of cranial suture complexity in the genus *Caiman* (Crocodylia; Alligatoridae). *Revista Brasileria de Biologia* 60:689–694.

O'Meara RN, Asher RJ. 2016. The evolution of growth patterns in mammalian versus nonmammalian cynodonts. *Paleobiology* 42:439–464.

Owen R. 1860. *Palaeontology: or, A systematic summary of extinct animals and their geological relations*. A. and C. Black.

Padian K, Horner JR, De Ricqlès A. 2004. Growth in small dinosaurs and pterosaurs: the evolution of archosaurian growth strategies. *Journal of Vertebrate Paleontology* 24:555–571.

Parrington FR. 1936. IV-On the tooth-replacement in theriodont reptiles. *Philosophical Transactions of the Royal Society of London. Series B, Biological Sciences* 226:121–142.

1003 Pavanatto AEB, Pretto FA, Kerber L, Müller RT, Da-Rosa ÁAS, Dias-da-Silva S. 2018.
1004 A new Upper Triassic cynodont-bearing fossiliferous site from southern Brazil, with
1005 taphonomic remarks and description of a new traversodontid taxon. *Journal of*
1006 *South American Earth Sciences* 88:179–196.
1007 Rasband WS. 1997. ImageJ.
1008 Ray S, Bandyopadhyay S, Bhawal D. 2009. Growth patterns as deduced from bone
1009 microstructure of some selected neotherapsids with special emphasis on
1010 dicynodonts: phylogenetic implications. *Palaeoworld* 18:53–66.
1011 Ray S, Botha J, Chinsamy A. 2004. Bone histology and growth patterns of some
1012 nonmammalian therapsids. *Journal of Vertebrate Paleontology* 24:634–648.
1013 Rayfield EJ. 2005. Using finite-element analysis to investigate suture morphology: a
1014 case study using large carnivorous dinosaurs. *The Anatomical Record Part A:*
1015 *Discoveries in Molecular, Cellular, and Evolutionary Biology: An Official Publication*
1016 *of the American Association of Anatomists* 283:349–365.
1017 Ross ST. 1978. Trophic ontogeny of the leopard searobin, *Prionotus scitulus* (Pisces:
1018 Triglidae). *Fish. Bull* 76:225–234.
1019 Ruta M, Botha-Brink J, Mitchell SA, Benton MJ. 2013. The radiation of cynodonts and
1020 the ground plan of mammalian morphological diversity. *Proceedings of the Royal*
1021 *Society B: Biological Sciences* 280. DOI: 10.1098/rspb.2013.1865.
1022 Sampson SD, Ryan MJ, Tanke DH. 1997. Craniofacial ontogeny in centrosaurine
1023 dinosaurs (Ornithischia: Ceratopsidae): Taxonomic and behavioral implications.
1024 *Zoological Journal of the Linnean Society* 121:293–337. DOI: 10.1111/j.1096-
1025 3642.1997.tb00340.x.

1026 Sanchez-Villagra MR. 2010. Developmental palaeontology in synapsids: the fossil
1027 record of ontogeny in mammals and their closest relatives. *Proceedings of the*
1028 *Royal Society B: Biological Sciences* 277:1139–1147.
1029 Schiesari L, Werner EE, Kling GW. 2009. Carnivory and resource-based niche
1030 differentiation in anuran larvae: implications for food web and experimental ecology.
1031 *Freshwater Biology* 54:572–586.
1032 Sidor CA. 2001. Simplification as a trend in synapsid cranial evolution. *Evolution*
1033 55:1419–1442.
1034 Starck JM. 1993. Evolution of avian ontogenies. In: *Current ornithology*. Springer, 275–
1035 366.
1036 Start D. 2018. Ontogeny and consistent individual differences mediate trophic
1037 interactions. *The American Naturalist* 192:301–310.
1038 Sues HD, Hopson JA. 2010. Anatomy and phylogenetic relationships of
1039 *Boreogomphodont jeffersoni* (Cynodontia: Gomphodontia) from the Upper Triassic
1040 of Virginia. *Journal of Vertebrate Paleontology* 30:1202–1220.
1041 Tanner JB, Zelditch ML, Lundrigan BL, Holekamp KE. 2010. Ontogenetic change in
1042 skull morphology and mechanical advantage in the spotted hyena (*Crocuta*
1043 *crocuta*). *Journal of Morphology* 271:353–365.
1044 Team RC. 2013. R: A language and environment for statistical computing.
1045 Thompson DW. 1942. On growth and form. *On growth and form.*
1046 To KHT, O'Brien HD, Stocker MR, Gignac PM. 2021. Cranial Musculoskeletal
1047 Description of Black-Throated Finch (Aves: Passeriformes: Estrildidae) with
1048 DiceCT. *Integrative Organismal Biology* 3:obab007.

1049 Toro-Ibacache V, Zapata MuÑoz V, O'higgins P. 2015. The predictability from skull
1050 morphology of temporalis and masseter muscle cross-sectional areas in humans.
1051 *The Anatomical Record* 298:1261–1270.
1052 Voje KL, Hansen TF, Egset CK, Bolstad GH, Pelabon C. 2014. Allometric constraints
1053 and the evolution of allometry. *Evolution* 68:866–885.
1054 Wang S, Stiegler J, Amiot R, Wang X, Du G hao, Clark JM, Xu X. 2017. Extreme
1055 Ontogenetic Changes in a Ceratosaurian Theropod. *Current Biology* 27:144–148.
1056 DOI: 10.1016/j.cub.2016.10.043.
1057 Watson DMS, Romer AS. 1956. A classification of therapsid reptiles.
1058 White HE, Clavel J, Tucker AS, Goswami A. 2020. A comparison of metrics for
1059 quantifying cranial suture complexity. *Journal of the Royal Society Interface*
1060 17:20200476.
1061 Wynd BM, Peecook BR, Whitney MR, Sidor CA. 2017. The first occurrence of
1062 *Cynognathus crateronotus* (Cynodontia: Cynognathia) in Tanzania and Zambia,
1063 with implications for the age and biostratigraphic correlation of Triassic strata in
1064 southern Pangea. *Journal of Vertebrate Paleontology* 37:228–239.
1065 Wynd BM, Uyeda JC, Nesbitt SJ. 2021. Including distorted specimens in allometric
1066 studies: linear mixed models account for deformation. *Integrative Organismal*
1067 *Biology*.
1068
1069

Figure Captions

FIGURE 1: Reconstruction of the skull of *Exaeretodon argentinus* indicating the measurements taken for this study. Reconstructions are based on MCZ VPRA-4483. The skull is shown in **A**) dorsal, **B**) ventral, and **C**) right lateral views. **Abbreviations**: **BB**, basicranial length; **BSL**, basal skull length; **BW**, maxillary bicanine width; **DL**, diastema length; **IO**, interorbital distance; **MUL**, muzzle length; **OD**, orbit diameter; **OL**, orbit length; **OW**, occipital plate width; **PAL**, palate length; **PD**, posterior postcanine distance; **SW**, skull width; **TEL**, temporal region length; **TP**, transverse process width; **UP**, upper postcanine tooth row length; **ZH**, zygoma height; **ZW**, maximum zygoma width.

FIGURE 2: Skull size does not correspond to degree of deformation. Number of deformed features is used as a proxy to compare degree of deformation between specimens, and there are no recovered relationships between size and overall cranial deformation.

FIGURE 3: Representative plots comparing the fit of the Generalized linear mixed effects model (GLMM), to the ordinary least squares regression. 95% confidence intervals are reported as dotted lines in corresponding colors. **A**) similar fit with overlapping confidence intervals. GLMM has confidence intervals that are more narrow than those for the ordinary regression. **B**) a similarly positive slope for both models with a poorly fit ordinary regression. **C**) contrasting slopes between models with an overall poor fit for both models, but the GLMM is able to incorporate specimens that indicate

1093 that the slope is not negative, which would be biologically unrealistic.

1094

1095 FIGURE 4: Reconstruction of ontogenetic change in the skull of *Exaeretodon*
1096 *argentinus*. Large specimen is based on MCZ VPRA-4483, and small specimen is
1097 based on MCZ VPRA-4470. Specimens are shown in **A**) ventral, **B**) dorsal, and **C**)
1098 ventral. Reconstructions are not reflective of actual size differences between individuals
1099 but are meant to indicate the major morphological differences between large and small
1100 individuals.

1101

1102 FIGURE 5: Sutural morphology in *Exaeretodon argentinus*. **A**) MCZ VPRA-4470 (BSL:
1103 166.6 mm) dorsal view of the interorbital region and posterior snout, with a simple
1104 contact between the nasals-frontals-prefrontals. **B**) MCZ VPRA-338-58M (BSL: 210.6
1105 mm) dorsal view of the interorbital region and posterior snout, showing simple sutural
1106 contacts between the nasals-frontals-prefrontals. **C**) MCZ VPRA-4483 (BSL: 305 mm)
1107 dorsal view of the interorbital region and posterior snout, with most sutural contacts
1108 occluded by matrix/breakages, but the nasofrontal suture is clearly interdigitated. **D**)
1109 MCZ VPRA-4483 lateral view of the orbit and anterior portion of the zygoma showing
1110 interdigitation between the postorbital-jugal contact. **E**) MCZ VPRA-4483 in dorsal view
1111 with interdigitated suture between the nasolacrimal anterolateral to the right orbit. **F**)
1112 MCZ VPRA-338-58M left zygoma in lateral view with simple, non-interdigitated contacts
1113 between the postorbital-jugal and jugal-squamosal. Scale bar equals 2 cm in all panels.

1114

1115 FIGURE 6. SEM images of a tooth cast, capturing the labial face of an isolated

postcanine tooth attributed to MCZ VPRA-4470. Central panel, line drawings of the upper left postcanine in distal and labial views (from top to bottom). Grey boxes in approximate location and are not exactly where the images are taken from. **A**) groove between primary (mesialmost) and secondary cusps, in the apicobasal midpoint of the cast; **B**) labialmost portion of the primary cusp; **C**) groove between primary and secondary cusps, just below the apical margin; **D**) area surrounding wear-facet (bottom left), located at the apical tip of the primary cusp. Arrows denote the mesial (anterior) direction, with striations (anisotropy) perpendicular to the mesiodistal axis of the tooth. Dark rounded areas are holes and are an artifact of bubbles in the casting material. SEM scale bar equals 1 mm.

Table 1(on next page)

Table 1: *Exaeretodon argentinus* specimen condition

1 Table 1: *Exaeretodon argentinus* specimen condition

Museum	***Specimen #***	***Skull length (mm)***	***Condition***	***In person/Photo?***
MACN	18125	443.6	Nasals broken dorsally, slight lateral shear	Photo
MACN	18193	231.7	Unprepared, lateral and ventral views not represented in photographs	Photo
MCZ VPRA	338-58M	210.6	Premaxilla missing	In person (BMW)
MCZ VPRA	4468	320	Dorsal surface encased in plaster with lateral shear	In person (BMW)
MCZ VPRA	4470	166.6	Premaxilla missing with lateral shear	In person (BMW)
MCZ VPRA	4472	202.6	Dorsal surface encased in plaster	In person (BMW)
MCZ VPRA	4478	156.1	Unprepared, right zygoma broken, left orbit broken, some anteroposterior crushing	In person (BMW)
MCZ VPRA	4483	305	Premaxilla missing, lateral shear primarily in zygomas	In person (BMW)
MCZ VPRA	4486	435	Braincase reconstructed with plaster	In person (BMW)
MCZ VPRA	4493	225	Lateral shear with displaced muzzle bones. Lower jaws fused to skull	In person (BMW)
MCZ VPRA	4494	265	Dorsal surface abraded	In person (BMW)
MCZ VPRA	4505	312.3	Right zygoma missing	In person (BMW)
MCZ VPRA	4781	149	Specimen used for thin-section, zygoma missing	In person (BMW)
PVL	2056	178	Mediolaterally crushed with left side abraded	In person (FA)
PVL	2067	294.3	Right side abraded with zygoma missing	Photo
PVL	2080	334.2	Right side abraded with zygoma missing	Photo
PVL	2082	265.7	Dorsoventrally crushed, dorsal braincase and part of the snout with plaster, left zygoma missing	In person (FA)
PVL	2085	330.8	Left zygoma missing, unprepared	Photo
PVL	2094	335	Portions of temporal area reconstructed with plaster	In person (FA)
PVL	2109	274.3	Mediolateral crushing with posterior shear, right zygoma missing	Photo
PVL	2473	328	Severe mediolateral crushing, left zygoma missing	In person (FA)
PVL	2554	330	Dorsal skull eroded, basicranium and both zygoma missing	In person (FA)
PVL	2565	230	Right anterior snout and zygoma missing	In person (FA)
PVSJ	103	495.9	Slight lateral shear, ventral view not represented in photographs	Photo

2

Table 2(on next page)

Table 2: Measurement definitions

*When elements are missing on one side, it is presented as the duplication of the measurement on one side of the skull

1 Table 2: Measurement definitions

Abbrv.	Feature	Measurement
BB	Basicranial length	Length from the posterior extent of occipital condyles to the anterior extent of the pterygo-paraoccipital foramen
BSL	Basal skull length	Tip of snout to the posterior extent of the occipital condyles
BW	Maxillary bicanine width*	Width of the snout, taken dorsally at the level of the canines
DL	Diastema length	Length from distal edge of canine to mesial edge of the first postcanine
IO	Interorbital distance*	Minimum distance between the orbits
MUL	Muzzle length	Tip of the snout to the anterior extent of the orbit
OD	Orbit diameter	Diameter of the orbit
OL	Orbit length	Anteroposterior length of the orbit
OW	Occipital plate width*	Maximum width between the opisthotics
PAL	Palate length	Tip of the snout to the posterior extent of the secondary palate
PD	Posterior postcanine distance*	Maximum width between the lingual margins of the distalmost postcanines
SW	Skull width*	Maximum width of the skull
TEL	Temporal region length	Posterior extent of lambdoidal crest to the anteriormost point of the temporal fenestra
TP	Transverse process width*	Maximum width between the lateral extent of the transverse processes.
UP	Upper postcanine length	Length of the postcanine series. Mesial and distal margins of alveoli are appropriate with missing teeth
ZH	Zygoma height	Maximum height of the zygoma, including both squamosal and jugal
ZW	Zygoma width	Lateralmost margin of squamosal to medial margin of the anteriormost tip of squamosal

2 *When elements are missing on one side, it is presented as the duplication of the measurement
3 on one side of the skull

Table 3(on next page)

Table 3: Summary statistics for Generalized linear mixed effects model (GLMM) and ordinary least squares regression (OLS)

GLMM used as the model to infer the allometric trends

n: the number of specimens used for the GLMM and OLS; ***D***: the number of distorted specimens coded for the GLMM; ***α***: slope of the regression line for both GLMM and OLS; ***β***: y-intercept for both GLMM and OLS; **P**; the p-value for if the regression line is significantly different from a line with a slope of 1; $\mathbf{R^2}$: the proportion of the data explained by the regression line under the OLS.

Table 3: Summary statistics for Generalized linear mixed effects model (GLMM) and ordinary least squares regression (OLS)

Feature	n_{GLMM}	D_{GLMM}	*Singular fit?*	α_{GLMM}	β_{GLMM}	*P (α = 1)*	n_{OLS}	α_{OLS}	β_{OLS}	*P (α = 1)*	R^2	*Trend*
MUL	22	14	false	0.96405	-0.27381	0.5516	8	0.9364	-0.1934	0.55	0.9243	Isometric
PAL	12	9	true	0.843915	0.005033	0.0792	3	0.9889	-0.329	0.937	0.9697	Isometric/Negative
OL	19	10	false	**0.7321**	-0.1688	**0.0248**	9	**0.564**	0.3006	**0.0234**	0.6203	**Negative**
IO	19	14	false	0.9488	-0.4668	0.73	5	0.6144	0.3495	0.329	0.4389	Isometric
TEL	20	12	true	**1.1761**	-0.8304	**0.0421**	8	1.2077	-0.8982	0.1487	0.9271	**Positive**
SW	21	12	false	1.13435	-0.39337	0.16	9	1.1553	-0.4326	0.379	0.8572	Isometric
BW	22	11	false	0.9877	-0.4419	0.916	11	1.1296	-0.8099	0.4736	0.8008	Isometric
UP	16	4	true	**0.5286**	0.6217	**0.000685**	12	**0.5026**	0.6808	**0.0025**	0.5845	**Negative**
PD	14	9	true	0.9652	-0.6719	0.836	5	1.4392	-1.8318	0.414	0.6902	Isometric
TP	12	10	false	0.83507	-0.12841	0.101	2	0.82948	-0.05587	0.175	0.9967	Isometric/Negative
OD	9	7	true	0.195	1.102	0.119	2	-0.8149	3.5133	0.575	0.1112	Isometric
OW	14	8	false	1.1273	-0.6721	0.3359	6	1.1978	-0.8085	0.461	0.824	Isometric
BB	12	5	true	**0.5238**	0.4759	**0.00606**	7	0.6402	0.2059	0.0966	0.6715	**Negative**
ZH	15	12	false	1.3084	-1.3293	0.08026	3	1.5675	-2.0717	0.0993	0.9704	Isometric/Positive
DL	14	11	false	1.1151	-1.2797	0.806	3	0.9384	-0.7213	0.905	0.678	Isometric
ZW	12	3	True	1.1894	-1.4933	0.623	9	1.059	0.4493	0.899	0.4098	Isometric

GLMM used as the model to infer the allometric trends

n: the number of specimens used for the GLMM and OLS; ***D***: the number of distorted specimens coded for the GLMM; ***α***: slope of the regression line for both GLMM and OLS; ***β***: y-intercept for both GLMM and OLS; **P**; the p-value for if the regression line is significantly different from a line with a slope of 1; $\mathbf{R^2}$: the proportion of the data explained by the regression line under the OLS.

Table 4(on next page)

Table 4: Allometric comparisons between cynodonts

Coefficients for *E. argentinus* are based on the GLMM, whereas coefficients for the other taxa are based on reduced major axis regression (data taken and adapted from Jasinoski & Abdala, 2017a)

*Marginally significant ($0.05 < p \lesssim 0.1$)

Abbreviations: Feature names are listed in Table 2; **Iso**, Isometry; **Neg**, Negative allometry; **Pos**, Positive allometry. Positive and negative allometries are colored green and red, respectively.

Table 4: Allometric comparisons between cynodonts

Feature	*Galesaurus planiceps*	*Thrinaxodon liorhinus*	*Diademodon tetragonus*	*Massetognathus pascuali*	***Exaeretodon argentinus***	*Chinquodon theotonicus*
MUL	Iso (0.94)	Pos (1.17)	Iso (1.01)	Neg (0.94)	Iso (0.96)	Iso (1.02)
PAL	Iso (0.96)	Pos (1.15)	Iso (0.98)	Neg (0.83)	Neg* (0.84)	Pos (1.12)
OL	Neg (0.63)	Neg (0.65)		Neg (0.91)	Neg (0.73)	Iso (0.97)
IO	Iso (1.09)	Iso (0.99)	Iso (0.92)	Iso (1.09)	Iso (0.95)	Iso (1.09)
TEL	Pos (1.96)	Pos (1.41)		Pos (1.25)	Pos (1.18)	Pos (1.12)
SW	Pos (1.56)	Iso (0.95)	Pos* (1.17)	Pos (1.30)	Iso (1.13)	Pos (1.12)
BW	Iso (1.09)	Iso (1.1)	Iso (1.02)	Iso (0.99)	Iso (0.99)	Pos (1.24)
UP	Iso (0.9)	Iso (0.93)	Neg (0.93)	Neg (0.83)	Neg (0.53)	Iso (0.93)
OD	Iso (1.02)	Neg (0.87)	Neg (0.69)	Neg (0.73)	Iso (1.1)	
OW	Iso (0.99)	Iso (0.9)	Pos (1.28)	Iso (1.12)	Iso (1.13)	Iso (1.11)
BB	Iso (0.73)	Iso (0.92)		Neg (0.87)	Neg (0.52)	Pos (1.28)
ZH	Pos (1.83)	Iso (1.17)	Pos (1.21)	Pos (1.37)	Pos* (1.31)	Pos (1.24)

Coefficients for *E. argentinus* are based on the GLMM, whereas coefficients for the other taxa are based on reduced major axis regression (data taken and adapted from Jasinoski & Abdala, 2017a)

*Marginally significant ($0.05 < p \lesssim 0.1$)

Abbreviations: Feature names are listed in Table 2; **Iso**, Isometry; **Neg**, Negative allometry; **Pos**, Positive allometry. Positive and negative allometries are colored green and red, respectively.

Table 5(on next page)

Table 5: Comparing hypothetical juveniles of *Exaeretodon argentinus* with *Diademodon tetragonus*

All values represent the ratio of a feature with total skull length, as a way to standardize measurements across differing body sizes. Hypothetical juveniles of *E. argentinus* are generated by multiplying Log_{10}(BSL) by the corresponding slope (α_{GLMM}) and adding the corresponding y-intercept (β_{GLMM}).

Table 5: Comparing hypothetical juveniles of *Exaeretodon argentinus* with *Diademodon tetragonus*

Feature	***Exaeretodon argentinus* (BSL: 20 mm)**	***Exaeretodon argentinus* (BSL: 40 mm)**	***Diademodon tetragonus* (MB.R 989; BSL: 189.2 mm)**
SW:BSL	0.60	0.66	0.90
TEL:BSL	0.25	0.29	0.40
ZH:BSL	0.12	0.15	0.39
ZW:BSL	0.06	0.07	0.11

All values represent the ratio of a feature with total skull length, as a way to standardize measurements across differing body sizes. Hypothetical juveniles of *E. argentinus* are generated by multiplying Log_{10}(BSL) by the corresponding slope (α_{GLMM}) and adding the corresponding y-intercept (β_{GLMM}).

Figure 1

Reconstruction of the skull of *Exaeretodon argentinus* indicating the measurements taken for this study.

Reconstructions are based on MCZ VPRA-4483. The skull is shown in **A**) dorsal, **B**) ventral, and **C**) right lateral views. **Abbreviations**: **BB**, basicranial length; **BSL**, basal skull length; **BW**, maxillary bicanine width; **DL**, diastema length; **IO**, interorbital distance; **MUL**, muzzle length; **OD**, orbit diameter; **OL**, orbit length; **OW**, occipital plate width; **PAL**, palate length; **PD**, posterior postcanine distance; **SW**, skull width; **TEL**, temporal region length; **TP**, transverse process width; **UP**, upper postcanine tooth row length; **ZH**, zygoma height; **ZW**, maximum zygoma width.

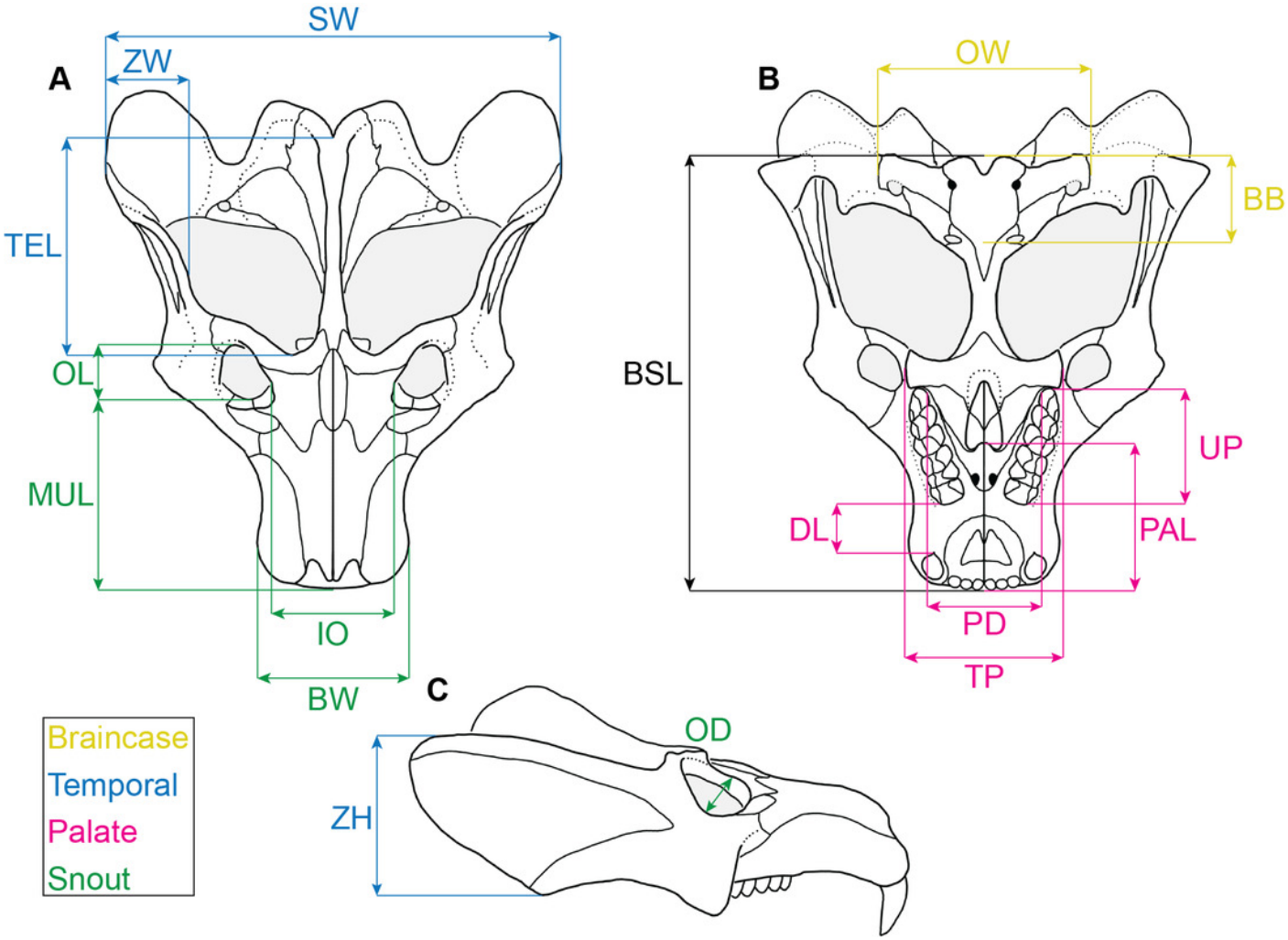
A
SW
ZW
TEL
OL
MUL
IO
BW
B
OW
BB
BSL
UP
DL
PAL
PD
TP
C
OD
ZH
Braincase
Temporal
Palate
Snout

Figure 2

Skull size does not correspond to degree of deformation.

Number of deformed features is used as a proxy to compare degree of deformation between specimens, and there are no recovered relationships between size and overall cranial deformation.

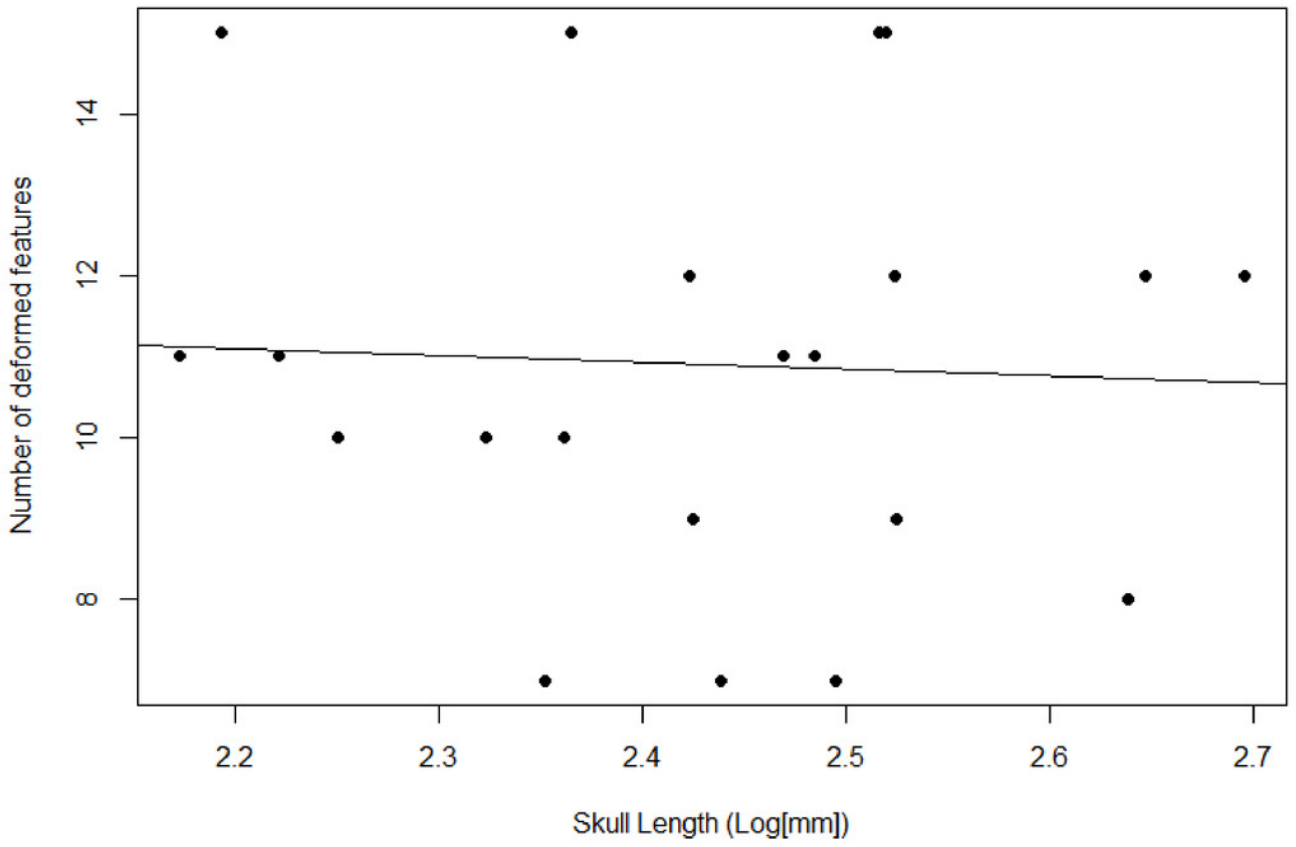

Figure 3

Representative plots comparing the fit of the Generalized linear mixed effects model (GLMM), to the ordinary least squares regression.

95% confidence intervals are reported as dotted lines in corresponding colors. **A**) similar fit with overlapping confidence intervals. GLMM has confidence intervals that are more narrow than those for the ordinary regression. **B**) a similarly positive slope for both models with a poorly fit ordinary regression. **C**) contrasting slopes between models with an overall poor fit for both models, but the GLMM is able to incorporate specimens that indicate that the slope is not negative, which would be biologically unrealistic.

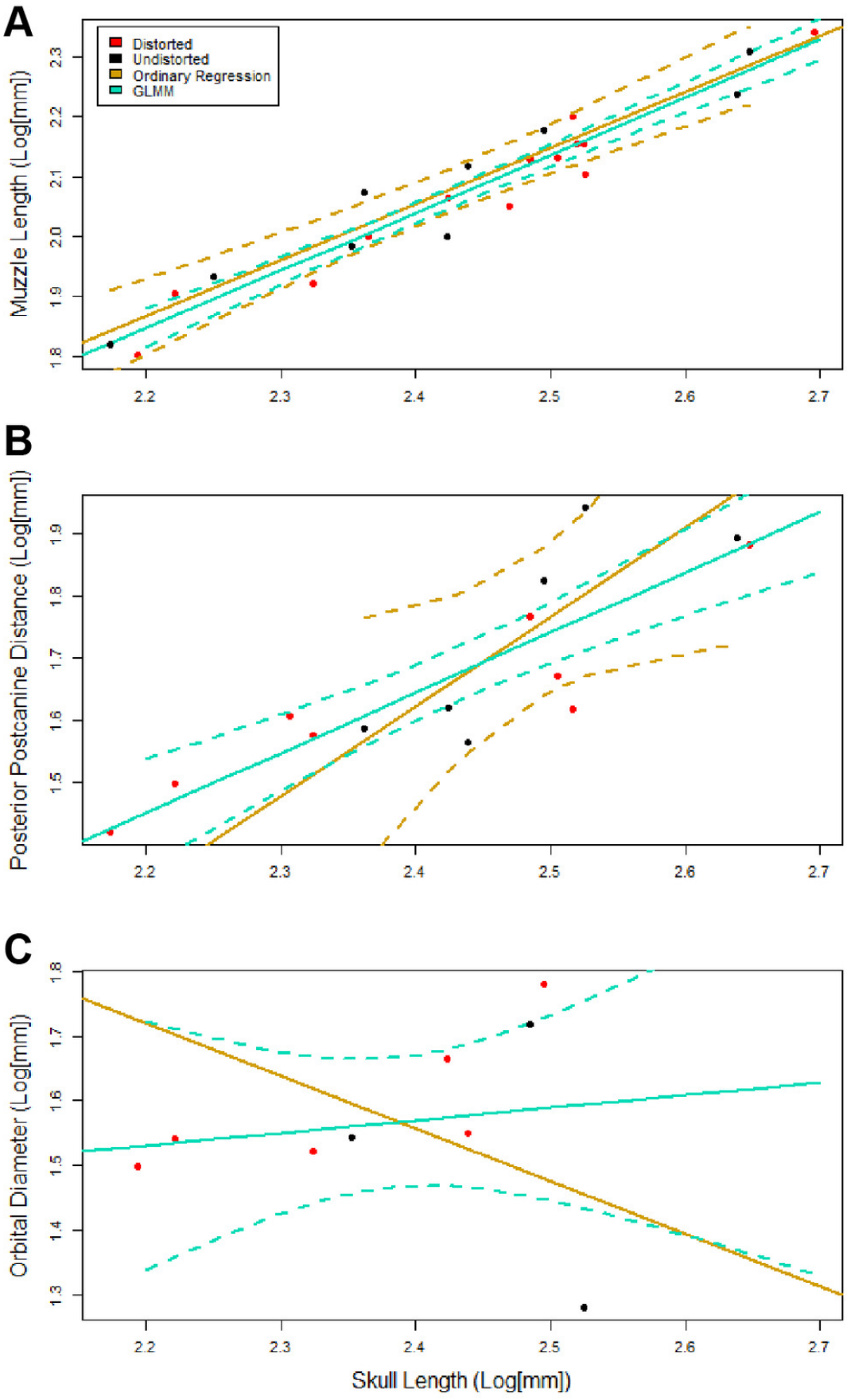
A
Distorted
Undistorted
Ordinary Regression
GLMM
Muzzle Length (Log[mm])
B
Posterior Postcanine Distance (Log[mm])
C
Orbital Diameter (Log[mm])
Skull Length (Log[mm])

Figure 4

Reconstruction of ontogenetic change in the skull of *Exaeretodon argentinus*.

Large specimen is based on MCZ VPRA-4483, and small specimen is based on MCZ VPRA-4470. Specimens are shown in **A**) ventral, **B**) dorsal, and **C**) ventral. Reconstructions are not reflective of actual size differences between individuals but are meant to indicate the major morphological differences between large and small individuals.

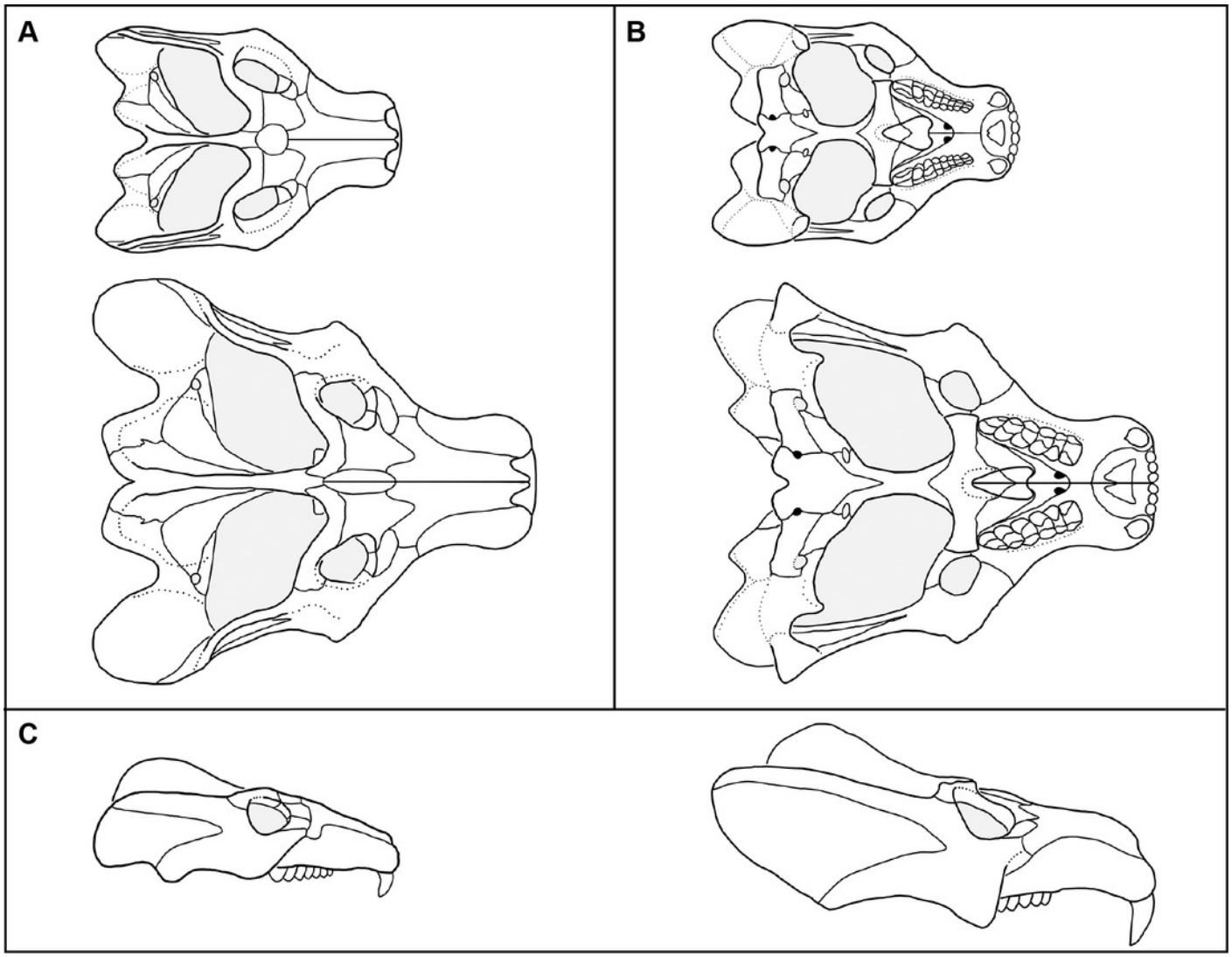

Figure 5

SEM images of a tooth cast, capturing the labial face of an isolated postcanine tooth attributed to MCZ VPRA-4470.

Central panel, line drawings of the upper left postcanine in distal and labial views (from top to bottom). Grey boxes in approximate location and are not exactly where the images are taken from. **A**) groove between primary (mesialmost) and secondary cusps, in the apicobasal midpoint of the cast; **B**) labialmost portion of the primary cusp; **C**) groove between primary and secondary cusps, just below the apical margin; **D**) area surrounding wear-facet (bottom left), located at the apical tip of the primary cusp. Arrows denote the mesial (anterior) direction, with striations (anisotropy) perpendicular to the mesiodistal axis of the tooth. Dark rounded areas are holes and are an artifact of bubbles in the casting material. SEM scale bar equals 1 mm.

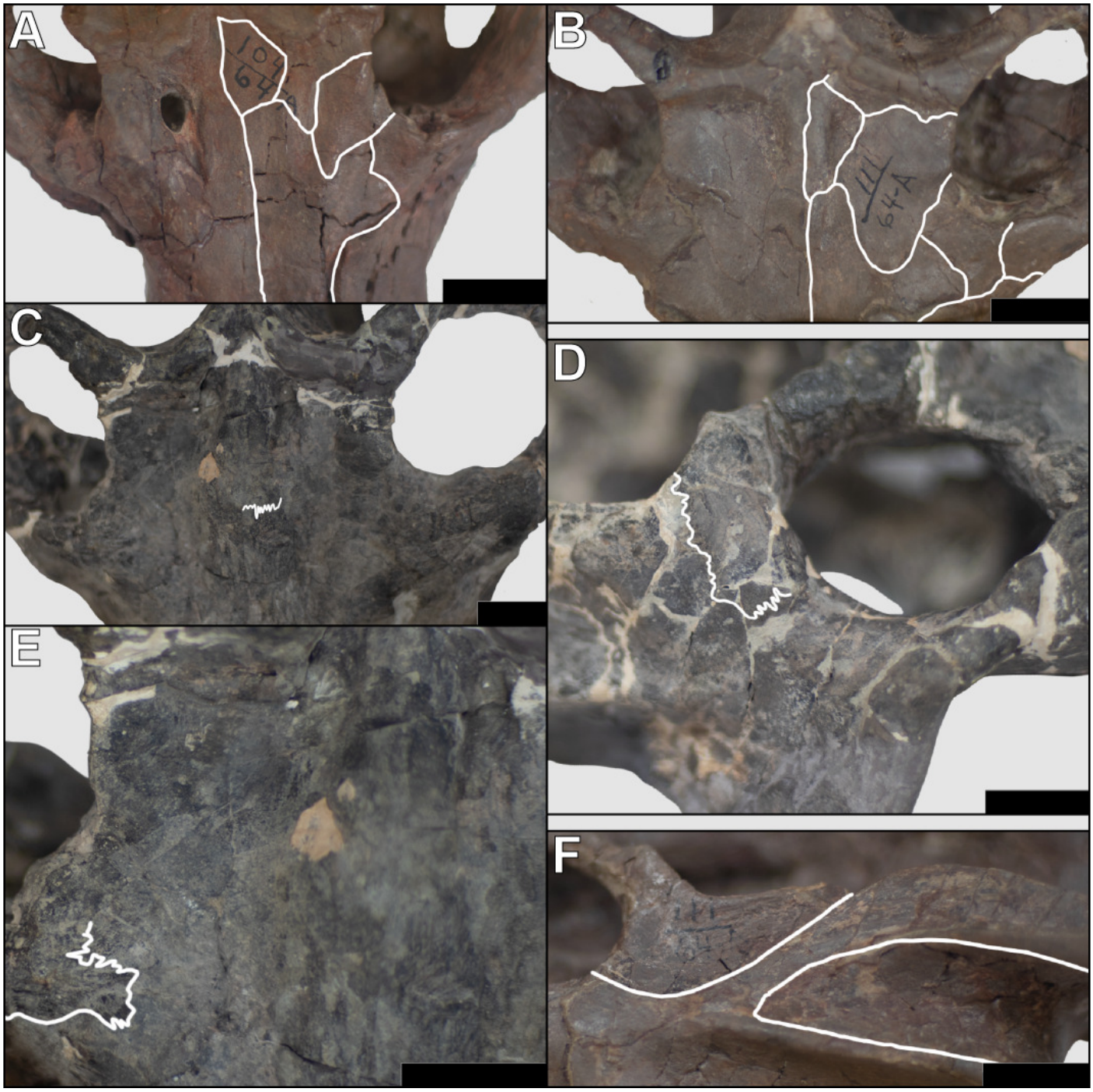
A
B
C
D
E
F

Figure 6

Sutural morphology in *Exaeretodon argentinus*.

A) MCZ VPRA-4470 (BSL: 166.6 mm) dorsal view of the interorbital region and posterior snout, with a simple contact between the nasals-frontals-prefrontals. **B**) MCZ VPRA-338-58M (BSL: 210.6 mm) dorsal view of the interorbital region and posterior snout, showing simple sutural contacts between the nasals-frontals-prefrontals. **C**) MCZ VPRA-4483 (BSL: 305 mm) dorsal view of the interorbital region and posterior snout, with most sutural contacts occluded by matrix/breakages, but the nasofrontal suture is clearly interdigitated. **D**) MCZ VPRA-4483 lateral view of the orbit and anterior portion of the zygoma showing interdigitation between the postorbital-jugal contact. **E**) MCZ VPRA-4483 in dorsal view with interdigitated suture between the nasolacrimal anterolateral to the right orbit. **F**) MCZ VPRA-338-58M left zygoma in lateral view with simple, non-interdigitated contacts between the postorbital-jugal and jugal-squamosal. Scale bar equals 2 cm in all panels.

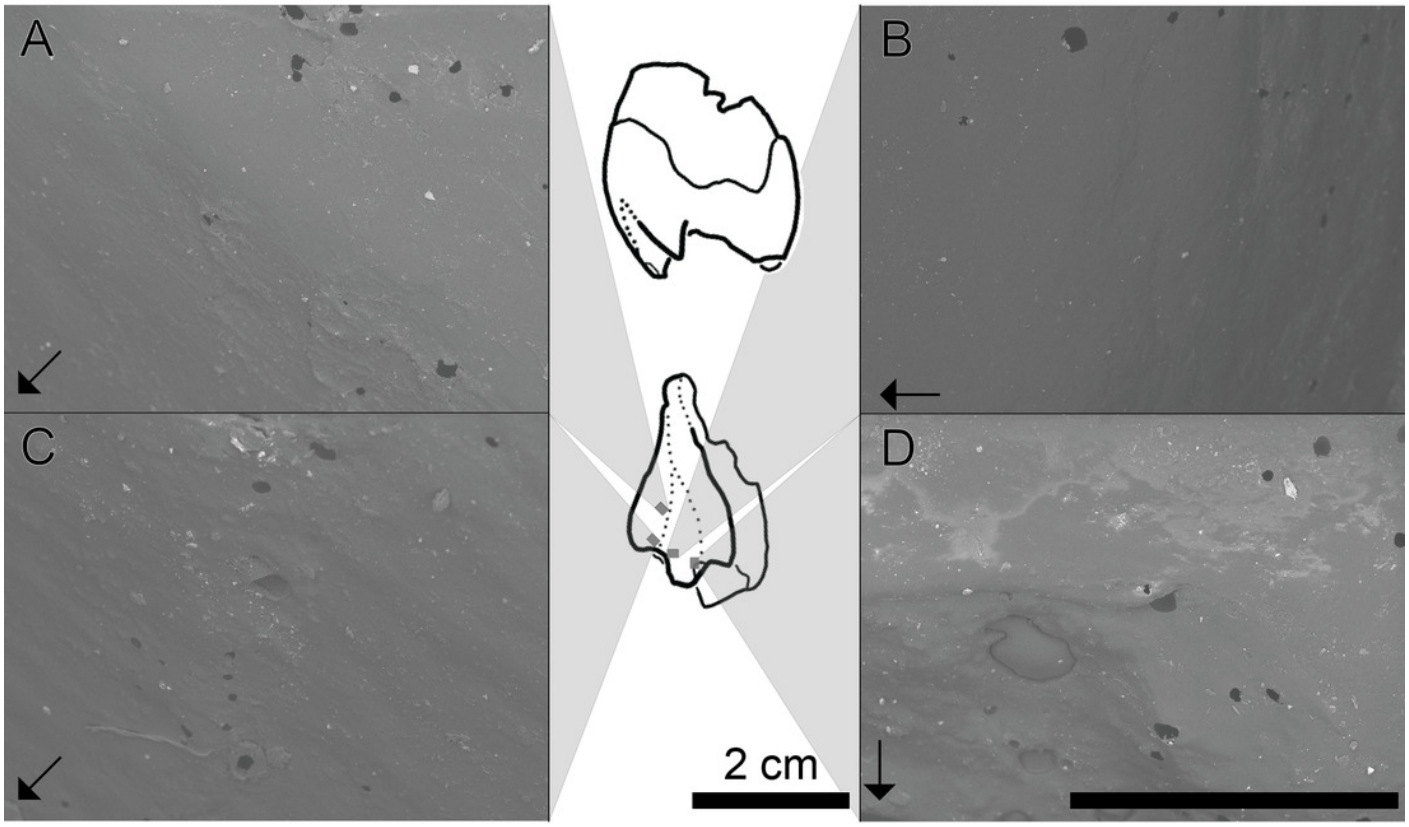
A
B
C
D
2 cm